Post print of: Molecular Human Reproduction, Volume 22, Issue 12, 1 December 2016, Pages 882–897,
https://doi.org/10.1093/molehr/gaw055
https://academic.oup.com/molehr/article/22/12/882/2354518

Differences in cumulus cell gene expression indicate the benefit of a pre-maturation step to improve in vitro bovine embryo production

Cecilia Dieci[1§], Valentina Lodde[1§], Rémi Labreque[2], Isabelle Dufort[2], Irene Tessaro[1,3], Marc-André Sirard[2] and Alberto M. Luciano[1]

[1]Reproductive and Developmental Biology Laboratory, Department of Health, Animal Science and Food Safety, University of Milan, 20133 Milan, Italy; [2]Centre de Recherche en Biologie de la Reproduction, Département des Sciences Animales, Université Laval, Québec, QC, Canada.

[§]Contributed equally

Key Words: oocyte, chromatin, follicle, granulosa cells, cumulus cells, apoptosis, pre-maturation, embryo development

Running Title: Cumulus cells gene expression and oocyte competence

Correspondence: Alberto M. Luciano, Dipartimento di Scienze Veterinarie per la Salute, la Produzione Animale e la Sicurezza Alimentare, Università degli Studi di Milano, Via Celoria, 10 - 20133 Milano, Italy - Phone (+39) 02 50317969 - alberto.luciano@unimi.it

[3]Present address: I.R.C.C.S. Istituto Ortopedico Galeazzi - Via R. Galeazzi, 4 – 20161 Milan (Italy).

Abstract

STUDY HYPOTHESIS The present study was designed to test the hypothesis that gene expression profile of cumulus cells (CC) isolated from oocytes with different degree of chromatin compaction within the germinal vesicle (GV) reflects oocyte quality and that each class of oocytes responds differently to the cultural environment during in vitro embryo production (IVP).

STUDY FINDING Transcriptomic profile of cumulus cells investment is related to oocyte competence and sets the stage for the development of customized pre-maturation strategies to improve IVP.

WHAT IS KNOWN ALREADY Oocytes complete the acquisition of their competence during antral follicle development. During this period, chromatin configuration within the GV changes dynamically and is indicative of oocyte's developmental potential. The interactions between somatic and germ cells are critical for the acquisition of oocyte competence and modulate chromatin morphology and function.

STUDY DESIGN, SAMPLES/MATERIALS, METHODS Bovine cumulus-oocyte complexes were isolated from 0.5-6 mm antral follicles. Surrounding CC were separated from oocyte and classified as GV0, GV1, GV2 and GV3 according to the degree of oocyte's chromatin compaction. RNA extracted from CC belonging to each group was amplified and hybridized on a bovine embryo-specific 44K Agilent slide (EmbryoGene). The CC_GV1, CC_GV2 and CC_GV3 classes were each hybridized against the CC_GV0, representing a stage of early oocyte differentiation with poor development competence. Data were normalized with Loess and fold changes of differentially expressed genes were determined with Limma procedure. Microarray data were validated using quantitative RT-PCR on selected targets. Microarray data were further analyzed through: 1) between-group analysis (BGA), which classifies the samples according to their transcriptomic profiles; 3) cluster analysis according to the expression profile of each gene using the mFuzz Bioconductor package; 4) Ingenuity Pathway Analysis (IPA) to study gene regulation pattern and predicted function.

Furthermore, CC belonging to each GV group were cultured for 3hrs and apoptotic cells were assessed by in situ FLICA Pan-Caspase Assay. Finally, based on the analysis of CC transcriptomic profiles and the relationship between morphological features of the COC and the oocyte chromatin configuration, a customized, stage dependent oocyte pre-maturation (pre-IVM) system was used as proof-of-concept of in vitro differentiation strategy, in order to improve oocyte developmental potential before IVM. For this purpose blastocyst rate and quality were assessed after in vitro maturation and fertilization of pre-matured oocytes.

MAIN RESULTS AND THE ROLE OF CHANCE Overall, qRT-PCR results of a subset of 5 selected genes (Thrombospondine-1, Serpine-2, regulator of G-protein signaling-2, inhibin alpha and solute carrier family 39 member-8) were consistent with the microarray data. Clustering analysis generated 16 clusters representing the main profiles of transcription modulation. Of the 5571 significantly differentially expressed probes, the majority (25.49%) best fitted with cluster #6 (down regulation between CC_GV0 and CC_GV1 and stable low levels in successive groups). IPA identified the most relevant functions associated to each cluster. Genes included in cluster #1 were mostly related to biological processes such as "cell cycle" and "cell death and survival", while genes included in cluster #5 were mostly related to "gene expression". Interestingly, "lipid metabolism" was the most significant function identified in cluster # 6, #9 and #12. IPA of gene lists obtained from each contrast individually (CC_GV0 vs. CC_GV1; CC_GV0 vs. CC_GV2; CC_GV0 vs. CC_GV3), which considered the fold change difference for each gene, revealed that the main affected function in each contrast was "cell death and survival". Importantly, IPA revealed that apoptosis is predicted to be inhibited in CC_GV1 and CC_GV2, while it is activated in CC_GV3. Caspase Assay results indicated that a low percentage of CC_GV0 are prone to undergo apoptosis, while it significantly increases in CC from oocytes with condensed chromatin, reaching the highest level in CC_GV3 (ANOVA, $p<0.05$). Finally, the tailored oocyte pre-maturation strategy based on the liaison between

morphological features of the COC and the oocyte chromatin configuration demonstrated that pre-IVM improved developmental capability of oocyte at early stages of differentiation (GV1 enriched COC) while was detrimental for oocytes at more advanced stage of development (GV3 enriched COC).

LIMITATIONS, REASONS FOR CAUTION This study was conducted in cow. Whether or not the results are applicable to human requests further elucidation. Embryo transfer experiments are required to determine if the tailored system improvement in blastocyst rates leads to increased live birth rates.

WIDER IMPLICATIONS OF THE FINDINGS The identification of multiple non-invasive biomarkers predictive of oocyte quality can greatly strengthen the pre-IVM approach aimed to improve IVM outcomes. This has important potential implications in treating human infertility as well as developing breeding schemes in domestic mammals.

LARGE SCALE DATA GEO series accession number GSE79886 (http://www.ncbi.nlm.nih.gov/geo/query/acc.cgi?acc=GSE79886).

STUDY FUNDING AND COMPETING INTEREST(S) Work supported in part by NSERC Strategic Network EmbryoGENE, Canada and in part by CIG - Marie Curie Actions-Reintegration Grants within the EU 7FP (n. 303640, "Pro-Ovum"). The authors declare no potential conflict of interest.

Introduction

In vitro embryo production (IVP) remains inefficient in both clinical applications of human reproduction and animal breeding. In particular, the development of suitable conditions for in vitro oocyte maturation (IVM) that support high quality egg production is a mayor challenge in assisted reproductive technologies (ART) (Smitz *et al.* , 2011). In bovine, although many attempts to increase the number of transferable embryos have been made in the last decades, the efficiency of IVP techniques, calculated as the proportion of immature oocytes aspirated from middle antral follicles (2-8 mm in diameter) that reach the blastocyst stage of embryonic development, is struggling to overcome a 35% threshold (Lonergan and Fair, 2008) unless very specific hormonal programming is used that can double such rate (Blondin *et al.* , 2002, Landry *et al.* , 2016, Nivet *et al.* , 2012). In fact, oocytes retrieved from non-treated animals reveal heterogeneous cellular and molecular features as well as distinct embryonic developmental capabilities (Blondin and Sirard, 1995, Pavlok *et al.* , 1992). On the other hand, it is well known that oocytes enclosed in early antral follicles (less than 2 mm in diameter) have not yet acquired the competence to spontaneously resume meiosis once isolated from the follicular compartment (Blondin and Sirard, 1995, Pavlok *et al.*, 1992); thus they are generally not used in standard IVP protocols.

The diversity of oocyte competences is mainly due to the intrinsic heterogeneity of the cohort of follicles from which cumulus-oocyte complexes (COC), to be subjected to standard IVP procedures, are isolated (Merton *et al.* , 2003, Vassena *et al.* , 2003). In cow, as in humans, only one egg is released at each reproductive cycle while the remaining follicles undergo atresia (Gougeon, 1986, Lussier *et al.* , 1987). It is widely accepted that one of the main factor that impairs oocyte ability to become an embryo in vitro is the precocious meiotic resumption that occurs when oocytes are isolated from the follicles. This, indeed, interrupts the

process of oocyte capacitation (Coticchio *et al.* , 2015, Gilchrist *et al.* , 2008, Hyttel *et al.* , 1997) and creates an asynchrony between the nuclear and the cytoplasmic events that are required for oocyte differentiation program before ovulation (Eppig *et al.* , 1994). In addition, a large proportion of these oocytes have already started an atretic process (Adams *et al.* , 2008, Gougeon, 1996, Monniaux *et al.* , 2014).

Oocyte quality heterogeneity is reflected in differences in large-scale configuration of the chromatin enclosed in the germinal vesicle (GV) of immature oocytes (reviewed in (De La Fuente, 2006, Luciano *et al.* , 2014, Luciano and Lodde, 2013, Zuccotti *et al.* , 2005). In cow, oocytes isolated from early and middle antral follicles present four patterns of chromatin configuration, from GV0 to GV3 characterized by a progressive increase in compaction (Lodde *et al.* , 2007), transcriptional silencing (Lodde *et al.* , 2008, Luciano *et al.* , 2011) and global DNA methylation (Lodde *et al.* , 2009). Notably, oocytes with a GV0 configuration (isolated from early antral follicles) display a very limited capability to resume meiosis, while virtually all the GV1, GV2 and GV3 oocytes (isolated from mid-antral follicles) are capable to reach the metaphase II (MII) stage in vitro, regardless their GV configuration (Lodde *et al.*, 2007). Instead, only a limited percentage of GV1 oocytes reached the blastocyst stage after in vitro fertilization (IVF), while GV2 and GV3 oocytes showed a significantly higher embryonic developmental potential (Lodde *et al.*, 2007). Thus, large-scale chromatin configuration is a marker of oocyte differentiation and competence.

It is clear that a better characterization of the molecular determinants of oocytes heterogeneity would be beneficial in understanding basic oocyte biology as well as in improving IVP efficiency. In this view, we have recently analyzed the transcriptomic profile of bovine oocytes with different chromatin configurations to identify mRNA modulations occurring in the oocyte during the GV0-to-GV3 transition, (Labrecque *et al.* , 2015). The present study aimed to expand this knowledge by assessing the transcriptomic profile of cumulus cells (CC) isolated from oocytes with

different chromatin configurations. In fact proper assessment of the oocyte ‘signature’ cannot overlook features of surrounding CC. It is very well established that CC plays a fundamental role in the modulation of oocyte competence acquisition: during folliculogenesis oocyte growth and differentiation rely upon the establishment of a microenvironment generated by bidirectional paracrine regulatory signals and intercellular heterologous gap junctions communications between oocytes and somatic cells are pivotal (Eppig, 2001, Gilchrist *et al.*, 2008, Matzuk *et al.* , 2002). Moreover, previous studies show that the tight association between oocyte and companion cumulus cells is required for the progressive suppression of transcriptional activity, chromatin remodeling and competence acquisition during the final phase of oocyte growth in mice (De La Fuente and Eppig, 2001), cows (Luciano *et al.*, 2011) and humans (Sanchez *et al.* , 2015).

Moreover, based on the results of the microarray analysis, in a second part of the study, we hypothesized that each class of oocytes responds differently to the cultural environment during IVP. To test this hypothesis, and considering that it is technically not possible to identify the chromatin configuration without DNA staining after removal of CC, we first looked for possible morphological markers that could be related to the chromatin configuration of the corresponding oocyte, and used these criteria to select a population of COC enriched in GV1 oocytes (which are the less competent when compared to GV2 and GV3). Then, on the basis of the microarray results, we designed a culture system specifically formulated to fulfill the specific needs of the oocyte in a specific stage and support their in vitro development. This system was used as proof-of-concept of in vitro differentiation strategy, the so-called "pre-maturation", in order to improve oocyte developmental potential before IVM. This in turn confirmed the hypothesis that each class of oocytes responds differently to the cultural environment during IVP.

Materials and methods

All chemicals and reagents were purchased from Sigma-Aldrich, unless otherwise stated.

Cumulus oocytes complexes (COC) collection

Ovaries were recovered at the abattoir (INALCA Spa, Ospedaletto Lodigiano, LO, IT 2270M CE, Italy) from 4-8 years old Holstein dairy cows and COC were retrieved from early (0.5-2 mm) and middle antral follicles (2-8 mm) as previously described (Lodde *et al.*, 2007). All the COC collected were then washed in medium 199 (M199) supplemented with HEPES 20 mM, 1790 units/L Heparin and 0.4% of bovine serum albumin (HM199) and examined under a stereomicroscope. Only COC suitable for standard *in vitro* embryo production procedures were used. Precisely only oocytes medium-brown in color, with homogenous or finely granulated ooplasm and surrounded by five or more complete layers of CC were included in the study, (Luciano *et al.* , 2005). The same morphological selection criteria are commonly accepted by the scientific community and applied in the commercial settings worldwide (Gordon, 2003, Stringfellow and Givens, 2010).

Cumulus cells isolation

COC were individually vortexed (2 min, 35 Hz) in HM199 supplemented with 5% of calf serum (Gibco, Thermo Fisher Scientific) to isolate cumulus cells (CC). In order to assess the chromatin configuration of oocytes corresponding to each cumulus, the denuded oocytes (DO) were individually washed in HM199, stained in HM199 containing 1 µg/mL Hoechst 33342 for 5 min in the dark, and then transferred into a 5 µL drop of the same medium, overlaid with mineral oil, and observed under an inverted fluorescence microscope (Olympus IX50, Olympus, magnification 40x). Oocytes were classified according to the degree of chromatin compaction within the

nuclear envelope as previously described (Lodde *et al.*, 2007): the GV0 stage is characterized by a diffuse filamentous pattern of chromatin in the whole nuclear area; the GV1 and GV2 configurations represent early and intermediate stages, respectively, of chromatin remodeling, a process starting with the appearance of few foci of condensation in GV1 oocytes and proceeding with the formation of distinct clumps of condensed chromatin in GV2 oocytes; the GV3, the stage where the maximum level of condensation is reached with chromatin organized into a single clump. For transcriptomic and gene expression analyses, CC isolated from each COC were individually collected in RNAse-free tubes, washed twice in cold PBS followed by centrifugation at 1000 rpm for 1 min at 4°C. After the removal of the supernatant, CC pellets (in the minimum volume of PBS possible) were snap-frozen in liquid nitrogen and stored at -80°C until RNA extraction. For the assessment of pan-Caspase activity, CC were isolated following the same experimental procedure with the exception that they were removed by pipetting to avoid cell damage. Then, CC isolated from a single COC were transferred into culture medium and assayed as described below.

RNA extraction

Groups of CC isolated from 10 oocytes with the same chromatin configuration were pooled and processed for total RNA extraction. Total RNA was extracted and purified with the Pico-Pure RNA Isolation Kit (ARCTURUS® - Thermo Fisher Scientific) following the manufacturer's protocol, with minor modification. Briefly, 10-30 µl of extraction buffer were added to each tube containing CC pellet from a single COC and incubated 30 minutes at 42 °C. Following incubation, extraction reaction mixtures from 10 tubes with CC isolated from oocytes bearing the same chromatin configuration were pooled and equal volumes of EtOH 70% were added to each tubes. Then, 250 µl of the RNA sample and EtOH mixture were loaded into the preconditioned purification columns and centrifuged for 2 minutes at 100 x g, this

step was repeated until all the RNA/EtOH mixtures were loaded into the columns. Finally, the columns were centrifuged at 16000 x g for 30 seconds to remove the flow-through and bind RNA. Following these steps, the procedure was performed according manufactures instructions and including DNase treatment (Qiagen) on the purification columns. A total of 4 pools for each chromatin configuration (CC_GV0, CC_GV1, CC_GV2 and CC_GV3) were used for microarray analysis and additional 4 pools for each chromatin configuration (from independent collections) were used for microarray validation by quantitative RT-PCR (qRT-PCR). Total RNA purity, integrity and concentration were evaluated using a 2100-Bioanalyzer (Agilent Technologies, Palo Alto, CA) with the RNA PicoLab Chip (Agilent Technologies). All extracted samples showed good quality with an RNA integrity number greater then 7.4.

RNA amplification, sample labeling and microarray hybridization

To generate enough material for the hybridization, RNA samples were linearly amplified according to the EmbryoGene pipeline. Antisense RNA (aRNA) was produced using the RiboAmp HS RNA amplification kit (Applied Biosystems, Thermo Fisher Scientific). After two amplification rounds of 6 hours each, the aRNA output was quantified using the NanoDrop ND-1000 (NanoDrop Technologies) (Gilbert *et al.* , 2009, Gilbert *et al.* , 2010). Then, for each sample, 4 µg of aRNA were labeled using the ULS Fluorescent Labeling Kit for Agilent arrays (with Cy3 and Cy5) (Kreatech Diagnostics, Amsterdam). The labeled product was then purified with the Pico-Pure RNA Isolation Kit. Labeling efficiency was measured using the Nano-Drop ND-1000. Samples from the four biological replicates, representing six different weeks of cumulus cells collection were hybridized on a custom bovine embryo specific Agilent 44K microarray slide (Robert *et al.* , 2011). The hybridizations were performed using a reference design, where cumulus cells isolated from oocytes bearing the GV1, GV2 or GV3 chromatin configuration where compared with CC isolated from GV0 oocytes (CC_GV0 vs. CC_GV1; CC_GV0 vs. CC_GV2; CC_GV0

vs. CC_GV3). Thus the reference group in the contrast is always represented by the CC_GV0 group. Overall, 12 hybridizations corresponding to the four biological replicates and three comparisons, were performed (figure 1A). A total of 825 ng of each labeled sample (Cy3 and Cy5) were incubated in a solution containing 10X blocking agent and 25X fragmentation buffer in a volume of 55 µL at 60°C for 15 min and were put on ice immediately after. Then, 55 µl of 2X GEx Hybridization Buffer HI-RPM were added for a total volume of 110 µl. The hybridization mix (100 µl) was added onto the array and hybridization was performed at 60°C for 17 hours using an Agilent Hybridization chamber in a rotating oven. After washing and drying steps, the slides were scanned using the Tecan PowerScanner microarray scanner (Tecan Group Ltd, Männerdorf, Switzerland) and features were extracted using ArrayPro 6.4 Analyzer (Media Cybernetics, Bethesda, MD).

Microarray data analysis

Microarray data analysis was performed according to the EmbryoGENE pipeline. Intensities files were uploaded to ELMA software (EmbryoGENE LIMS Microarray Analysis, http://elma.embryogene.ca/), to run the quality control module.

To detect the presence or absence of the signal for each spot present on the slide, microarray datasets generated by ELMA were analyzed and an arbitrary cut-off corresponding to the mean intensity of the background level plus twice the Standard Deviation (SD) of the background was used. A Venn diagram was created using the online tool VENNY to show present and common probes between groups. Moreover, a between-group analysis (BGA) was performed to classify the samples according to their transcriptomic profiles (Culhane *et al.* , 2002).

To calculate the gene expression fold change for each contrast individually (CC_GV0 vs. CC_GV1; CC_GV0 vs. CC_GV2; CC_GV0 vs. CC_GV3) microarray datasets generated by ELMA were analyzed with the FlexArray microarray analysis

software, Version 1.6.1 (Blazejczyk *et al.* , 2007). Briefly, raw data were subjected to a simple background subtraction, normalized within each array (Loess) and A Limma simple analysis was performed to obtain the fold change values. The reference group in the contrasts is represented by the CC_GV0 group.

In addition, datasets generated by ELMA were subjected to microarray analysis of variance (MAANOVA) that was conducted considering the four experimental groups and by using the CC_GV0 as reference group. Differences were considered statistically significant with a *P* value less than 0.05. After MANOVA analysis, probes were grouped in clusters according to their expression profile using the mFuzz Bioconductor package (Kumar and M, 2007).

Finally, the gene lists generated by our analysis were examined using Ingenuity Pathway Analysis (Ingenuity Systems, Mountain View, CA). All statistically significant genes (P-value <0.05) were uploaded to the application. The functional analysis identified the biological functions that were most significant to the molecules in the database.

cDNA preparation and quantitative RT-PCR

The validation of microarray results was performed by *quantitative* RT-PCR (qRT-PCR) using four independent biological replicates (each pool containing CC derived from 10 COC). For each sample, 1 ng of total RNA were reverse transcribed using the SuperScript First-Strand Synthesis for RT-PCR (Invitrogen - Thermo Fisher Scientific) with oligo-dT primers following the manufacturer's recommendations. Primer sequences used for real time RT-PCR are provided in supplemental table 1. Primers were designed using the Primer3 online tool (http://primer3.ut.ee/) from sequences obtained using the UMD3.1 assembly of the bovine genome. Specificity of each primers pair was confirmed by electrophoresis analysis on a standard 2% agarose gel and sequencing analysis.

The PCR products were purified with the QIAquick PCR Purification kit (Qiagen), quantified using the Qbit 2.0 fluorometer and Qubit dsDNA HS Assay Kit (Invitrogen - Thermo Fisher Scientific). Serial dilutions of the PCR products (ranging from 2 x 10^{-4} to 2 x 10^{-8} ng/µL) were then used to create the standard curves for the evaluation of the amplification efficiencies. Quantitative real-time PCR was performed on an iQ5 (Bio-Rad) using SYBR incorporation. Each qPCR reaction, in a final volume of 20 µL, contained the cDNA corresponding to 1ng of RNA extracted, 0.1 µM of each primer and 1x SYBR mix (iTaq Universal SyBR Green Supermix, Bio-rad). The PCR conditions used for all genes were as follows: a denaturing step of 30 sec at 95°C, followed by 40 PCR cycles (95°C for 30 sec; 57°C for 1 min), a melting curve (55°C for 1 min and a step cycle starting at 55°C, up to 94,5°C). PCR specificity was confirmed by melting-curve analysis.

For each gene tested, four independent biological replicates were used. Analysis of gene expression stability over the four groups was performed using the GeNorm algorithm (Vandesompele *et al.* , 2002) through the Biogazelle's qBase+ software (Biogazelle, Zwijnaarde, Belgium). Beta actin (ACTB), glyceraldehyde-3-phosphate dehydrogenase (GAPDH) and hypoxanthine phosphoribosyl transferase 1 (HPRT1) were identified as the most stable genes among the different groups, with M-value <1.5, and thus used as reference genes. Complementary DNA quantification was performed with the iQ5 Optical System Software Version 2.0 (Bio-Rad) using the delta delta Ct method, where CC form GV0 was used as reference group.

Active Caspase-positive cells analysis

Dispersed CC preparation (Luciano *et al.* , 2000) isolated from single oocytes with different chromatin configuration (CC_GV0, CC_GV1, CC_GV2 and CC_GV3) were collected as described above and processed through the *CaspaTag™ Pan-Caspase In Situ Assay Kit* (Merck Millipore, Billerica, MA, USA), a methodology

based on Fluorochrome Inhibitors of Caspases (FLICA) to detect active Caspase in cells undergoing apoptosis, following the manufacturer's specification sheet with slight modifications. Briefly, dispersed cumulus cells were plated in 4-well plate for 3 hours in TCM199 supplemented with 0.68 mM L-glutamine, 25 mM $NaHCO_3$, 0.2 mM sodium pyruvate and 0.4% fatty acid free BSA at 38.5°C and 5% CO_2, to allow them to adhere to the plate. Subsequently, cells were cultured for one additional hour in the presence of a carboxyfluorescein-labeled inhibitor of Caspases. After washings and fixation in 10% formaldehyde, cells were detached by gently pipetting and moved on a glass slide. When dried, cells were covered with the antifade medium Vecta Shield (Vector Laboratories, Burlingame, CA, USA) supplemented with 1 µg/ml 40,6-diamidino-2-phenylindole (DAPI) and analyzed under fluorescent microscopy (Nikon Eclipse E600). For each sample, 10/15 fields were randomly chosen and results were expressed as the number of active Caspase-positive cells over the total number of cells observed.

Assessment of the relationship between COC features and oocyte chromatin configuration.

In order to establish morphological criteria that would allow for the collection and /or selection of a population of COC enriched in one of the three GV chromatin configurations (GV1, GV2 or GV3), the relationship between the oocyte chromatin configuration and either 1) the size of the follicle from which the COC was isolated or 2) the morphology of the corresponding COC, were assessed.

To this aim, in a first set of experiments, follicle's sizes were determined with a ruler by measuring their visible diameter on the surface of the ovary. COC were collected from 2-4 mm, 4-6 or >6 mm antral follicles. In the second set of experiments, COC were collected from 2-8 mm antral follicles. In any case, only COC suitable for standard IVP procedure were included in the study. After the first selection, COC were further divided in three groups on the basis of morphological

characteristics previously described (Blondin and Sirard, 1995, Hazeleger *et al.* , 1995): Class 1, with homogeneous ooplasm and compact cumulus cells; Class 2, with minor granulation of the ooplasm with compact cumulus cells; Class 3, with highly granulated ooplasm and slight expansion of cumulus cells layers (Figure 6B) (Gordon, 2003, Stringfellow and Givens, 2010).

In both cases, COC were finally denuded and fixed in a methanol and Dulbecco's Phosphate-Buffered Saline (DPBS) solution (60:40), stained with DAPI for the assessment of chromatin configuration under fluorescence microscopy as above described.

Glucose-6-phosphate dehydrogenase (G6PDH) activity determination by brilliant Cresyl Blue (BCB) Staining

COC isolated from 2-8 mm antral follicles and selected as above described were separated into two groups based on the morphological criteria as Class 1 and Class 2/3 (Figure 6B). COC were then stained with BCB as previously described (Torner *et al.* , 2008), with slight modifications. Briefly, COC were incubated in 26 µM BCB diluted in DPBS with calcium and magnesium, and supplemented with 0.4% of BSA for 90 min at 38.5 °C in humidified air atmosphere. After washing, CC were removed and oocytes were examined under a stereomicroscope. Oocytes were classified as BCB negative (BCB-), when the oocyte showed a colorless cytoplasm, or BCB positive (BCB+) where oocytes showed different grades of blue/violet color (BCB+).

In vitro pre-maturation (pre-IVM), in vitro maturation (IVM), in vitro fertilization (IVF) and embryo culture (IVC)

For in vitro embryo production experiments, only COC from 2-8 mm middle antral follicles collected as above described were used. After isolation and selection, COC were divided based on the morphological criteria as Class 1, Class 2 and class

3 as above described. Groups of 20-30 COC belonging to Class 1, Class 2/3 or unsorted COC (a mix of Class1, Class 2 and Class 3, corresponding to the population of COC that is commonly used in standard IVP procedures) were subjected to standard IVP (IVM, IVF and IVC) with or without a pre-IVM culture step (Franciosi *et al.* , 2014). To avoid meiotic resumption before pre-IVM, COC were classified in HM199 supplemented with the non-selective PDE inhibitor 3-isobutyl-1-methyl-xanthine (IBMX) at the final concentration of 0.5 mM (Lodde *et al.* , 2013). Pre-IVM consisted of culture for 6 hours in M-199 added with 0.68 mM L-glutamine, 25 mM $NaHCO_3$, 0.4% BSA fatty acid free, 0.2 mM sodium pyruvate, 10^{-4} IU/ml of r-hFSH (Gonal-F, Serono, Rome, Italy) and 10 μM cilostamide in humidified air under 5% CO_2 at 38.5°C (Franciosi *et al.*, 2014).

For IVM, COC (immediately after collection or after 6h of pre-IVM) were cultured for 22 h in M-199 added with 0.68 mM L-glutamine, 25 mM NaHCO3, 0.4% BSA fatty acid free, 0.2 mM sodium pyruvate and 0.1 IU/ml of r-hFSH (Gonal-F, Merck Serono, Darmstadt, Germany) at 38.5°C in 5% CO_2 as described in (Luciano *et al.*, 2005).

IVF and IVC were carried out as previously described (Luciano *et al.*, 2005). At the end of culture period (d+8), the blastocyst rate was assessed under a stereomicroscope. The embryos were then fixed in 60% methanol in DPBS and the cell nuclei counted under a fluorescence microscope after staining with 0.5 mg/ml of propidium iodide (Luciano *et al.*, 2005).

Statistical analysis

Experiments were repeated at least 3 times. Data were analyzed by one-way ANOVA followed by Newman-Keuls Multiple Comparison test using Graph Pad Prism version 6.0h. Data are presented as mean ± SEM. P values <0.05 were considered statistically significant. For each experiment, the specific test used is indicated in the figure legend.

Results

Microarray results

To gain insights into transcriptomic profiles of CC associated to oocytes with different large-scale chromatin configurations, three microarray comparisons using the EmbryoGENE bovine microarray were performed. This microarray includes 42242 probes, of which 31138 represent reference genes, novel untranscribed region, 3'-untranslated region variants and alternatively spliced exons (Robert *et al.*, 2011).

As shown in **Figure 1A**, the hybridizations were performed using a reference design, where the CC isolated GV1, GV2 or GV3 chromatin configuration where compared with CC from GV0 oocytes (CC_GV0 vs. CC_GV1; CC_GV0 vs. CC_GV2; CC_GV0 vs. CC_GV3, the reference group in the contrast is represented by the CC_GV0 group. Microarray data were deposited in the National Center for Biotechnology Information (NCBI)'s Gene Expression Omnibus (Edgar *et al.* , 2002), and are accessible through GEO series accession number GSE79886 (http://www.ncbi.nlm.nih.gov/geo/query/acc.cgi?acc=GSE79886).

Considering the threshold used to detect the presence/absence of the spots on the microarray slides, a total of 20155 probes resulted to be commonly expressed in all the four groups (**Figure 1B**), while 384, 1138, 949 and 827 were expressed only in CC_GV0, CC_GV1, CC_GV2 and CC_GV3 respectively. As shown in **Figure 1C**, the BGA revealed the global transcriptional differences among CC isolated from oocytes with different chromatin configurations. Considering the biological replicates (dots) within each group, the CC_GV0 and CC_GV1 groups displayed more variation (increased distance between the dots) compared to GV2 and GV3. Moreover, CC_GV0 and CC_GV3 groups were characterized by unique gene expression profiles, while some minimal overlapping existed between CC_GV1 and CC_GV2 groups.

The MAANOVA algorithm revealed that 5571 probes were significantly differentially expressed ($p<0.05$) between groups, of which 112, 127 and 204 presented a fold change difference more than ±2 in CC_GV0 vs. CC_GV1, CC_GV0 vs. CC_GV2 and CC_GV0 vs. CC_GV3 respectively (**Table 1**). Clustering analysis with the mFuzz Bioconductor package generated 16 clusters representing the main profiles of transcription modulation (**Figure 2**). Of the 5571 significantly differentially expressed probes, 25.49 % best fitted with cluster # **6** profile (down regulation between CC_GV0 and CC_GV1 and relatively stable low levels in successive groups). Clusters #**1** (constant decrease from CC_GV0 to CC_GV3), cluster # **5** (constant increase from CC_GV0 to CC_GV3), cluster # **9** (up regulation between CC_GV0 and CC_GV1 and relatively stable levels in successive groups) and cluster # **12** (up regulation from CC_GV0 to CC_GV2 and relatively stable levels from CC_GV2 to CC_GV3) each included around 10% of the total probes, while the other clusters included a low number of probes (**Figure 2**).

A subset of 5 genes was selected, according to their significant changes in the three comparisons after Flex Array analysis and their known biological functions, to validate the microarray results by qRT-PCR. The chosen genes were: Thrombospondine 1 (THBS1), Serpine 2, regulator of G-protein signaling 2 (RGS2), inhibin alpha (INHA) and solute carrier family 39, member 8 (SLC39A8, **Supplemental table 1**). Overall, qRT-PCR results were consistent with the microarray data (**Figure 3**).

IPA based Functional Analysis

Lists of genes that best fitted each of the main clusters (#1, #5, #6, #9 and #12) were submitted to IPA in order to identify the most relevant molecular and cellular functions associated to each cluster (**Table 2**). The genes included in cluster 1 were related to biological processes such as ‘cell cycle’ and ‘cell death and survival’, while genes included in cluster #5 were more related to molecular

processes such as ‘gene expression’, ‘RNA post transcriptional modification’ and ‘protein synthesis’. Interestingly, ‘lipid metabolism’ and ‘small molecule biochemistry’ were the most significant functions identified in clusters # 6, #9 and #12.

Moreover, in order to gain insights into the molecular and cellular pathways that were likely affected in CC during oocyte chromatin compaction, gene lists obtained from each contrast individually by Flexarray (CC_GV0 vs. CC_GV1; CC_GV0 vs. CC_GV2; CC_GV0 vs. CC_GV3) were uploaded to IPA and analyzed considering the fold change difference for each gene. Interestingly one of the main affected functions in each contrast was ‘cell death and survival’ (**Table 3)**. Moreover, as shown in **Figure 4**, the number of apoptosis-related genes that were deregulated increased substantially from CC_GV0 vs. CC_GV1 to CC_GV0 vs. CC_GV3 contrasts. Importantly, IPA analysis revealed that apoptosis is predicted to be inhibited in CC_GV1 and CC_GV2, while it is activated in CC_GV3 (**Figure 4**, gene lists shown in figure 4 are provided as s**upplemental table 2**)

Active Caspase-positive cells analysis

In order to validate the in silico functional prediction (generated by IPA) that CC_GV3 are more prone to apoptosis, we analyzed the susceptibility of CC isolated from oocytes with different chromatin configuration to undergo apoptosis.

It has been shown that apoptotic cell death of granulosa cells is the molecular mechanism underlying follicle atresia (Jolly *et al.* , 1994). A previous study demonstrated that the dissociation of both mural granulosa cells and cumulus cells triggers apoptosis in both cell subsets (Luciano *et al.*, 2000). Therefore we used CC dissociation as a ‘stress test’ in order to assess whether chromatin compaction (from GV0 to GV3) was associated to an increased tendency of the oocyte’s associated CC to undergo apoptosis. CC isolated from single oocytes with different chromatin configurations (CC_GV0, CC_GV1, CC_GV2 and CC_GV3) were isolated and in

vitro cultured for 3 h and then assayed for Pan-Caspase activity. As shown in **Figure 5**, the percentage of Caspase positive cells was significantly lower in CC from GV0 oocytes, whereas it increased in CC from GV1 and GV2 oocytes, reaching the highest value in CC from GV3 oocytes, as predicted by IPA.

Assessment of the relationship between COC features and oocyte chromatin configuration.

The findings that CC isolated from oocytes with different chromatin configuration differ in their transcriptomic profiles and in their susceptibility to undergo apoptosis, lead us to hypothesis that COC isolated from middle antral follicles bearing oocytes with different chromatin configurations (GV1, GV2 or GV3) could respond differently to specific in vitro cultural conditions.

To test this hypothesis, and considering that it is technically not possible to directly identify the chromatin configuration without DNA staining after CC removal, we first looked for possible morphological markers that could be related to the chromatin configuration of the corresponding oocyte, and that therefore could be used to isolate a population of COC from middle antral follicle enriched in one of the GV stages (GV1, GV2 or GV3). Precisely, we considered the possible relationship between chromatin configuration and 1) the size of the follicle and 2) the morphology of the COC, using morphological criteria commonly accepted by the scientific community and clearly recognizable under a stereomicroscope. These studies revealed a relationship between the oocyte chromatin configuration and the morphology of the COC but not with the size of the follicle from which they originate (**Figure 6**). In fact, oocytes with GV1, GV2 and GV3 chromatin configuration were equally distributed in follicle of 2-4, 4-6 and > 6 mm in diameter (**Figure 6A**). On the other hand, as shown in **Figure 6B**, when isolated and additionally sub-grouped into 3 classes based on their morphology (Blondin and Sirard, 1995), Class 1 COC (with homogeneous ooplasm and compact cumulus cells) was the only one in which

oocytes with GV1 chromatin configuration could be found, while oocytes with GV1 chromatin configuration were almost absent in Class 2 and 3 COC (minor granulation of the ooplasm with compact cumulus cells, or highly granulated ooplasm and/or few outer layers cumulus cells showing expansion in Class 2 and 3 respectively),

Furthermore, BCB staining of Class 1, 2 and 3 COC indicated that Class 1 COC are in an earlier stage of differentiation when compared with Class 2 and 3 COC, giving additional (indirect) confirmation that chromatin compaction is associated with oocyte (and accompanying CC) differentiation. Indeed as shown in **Figure 6C**, the percentage of BCB- oocytes was significantly higher in Class 1 than Class 2/3 COC ($P<0.05$).

Effect of pre-IVM treatment on oocyte developmental competence

Having established that Class 1 and Class 2/3 COC differ in the relative percentage of oocytes with different chromatin configuration, and that Class 1 was the solely Class enriched with GV1 oocytes, we tested the hypothesis that these Classes respond differently to specific in vitro cultural conditions.

As shown in **Figure 7**, when subjected to standard IVP procedures (with regular IVM protocol) Class 1 COC showed a limited embryonic developmental competence (**Figure 7**). Indeed after 7 days of culture both blastocyst rate and mean blastocyst cell number per embryo were significantly lower in Class 1 COC when compared to Class 2/3 group ($p<0.05$). As expected, the group composed of the mix of Class 1, 2 and 3 COC, which correspond to the unsorted group of COC commonly used in IVP protocols, showed intermediate values between Class 1 and Class 2/3 COC. On the other hand, pre-IVM treatment increased significantly the developmental capability (blastocyst rate and mean blastocyst cell number per embryo) of Class 1 COC, had no effect on the mixed group, while it reduced the developmental competence of Class 2/3 COC.

Discussion

The present work provides the first comprehensive transcriptome analysis of bovine CC associated to oocytes with a specific large-scale chromatin configuration. This is particularly relevant as chromatin configuration is indicative of the state of oocyte differentiation in the antral follicle before dominance emergence in naturally cycling animals (Lodde *et al.*, 2007, Lodde *et al.*, 2008, Lodde *et al.*, 2009). Transcriptomic data analysis confirmed the hypothesis that features of the cumulus oophorus investment change along with oocyte chromatin compaction. Interestingly, results of the BGA analysis, that gives information on the overall transcriptomic profile of each biological sample, are in accordance with the global change in distribution of transcriptomic data obtained from oocytes with different chromatin configurations (compare Figure 1C of the present study and Figure 2 in Labrecque et al., 2015 (Labrecque *et al.*, 2015)). Collectively these data, and in particular the relative distance between each group, effectively confirms that global transcriptional differences exist among oocytes with different chromatin configurations as well as in their surrounding CC. Thus, the transcriptome of the whole cumulus-oocyte complex changes along with the increase in chromatin compaction.

According to our previous morphological and functional studies, the present clustering analysis of microarray data revealed that major changes in terms of CC transcripts differences occur during the GV0-to-GV1 transition (**Figure 2**). Indeed the cluster profiles # **6 and 9** (down or up regulation between CC_GV0 and CC_GV1 and relatively stable low levels in successive groups) collect about 36% of the differentially expressed probes. Interestingly, *in silico* functional analysis through IPA of the subsets of genes that best fitted with these two profiles, revealed a major change of CC transcripts involved in lipid metabolism during the GV0-to-GV1 transition. Recent works showed that the lipid content in CC reflect the quality of the female gamete (Auclair *et al.* , 2013, Montani *et al.* , 2012) both in human (Matorras

et al. , 1998) and in bovine (Kim *et al.* , 2001). It has been also recently reported that CC are able to protect the oocyte by storing elevated levels of free fatty acids from follicular fluid (Aardema *et al.* , 2013). In addition, studies in mice revealed that oocytes are deficient in cholesterol production and require CC to provide products of the cholesterol biosynthesis pathway, and suggest that oocytes promote cholesterol biosynthesis in CC through oocyte derived paracrine factors, probably to compensate their deficiency (Su *et al.* , 2008). Altogether these data sustain the general idea that defective lipid metabolism inside the COC may be in part responsible for the lower meiotic and developmental competence of the oocyte. In this view, we can speculate that CC acquire the "competence" of metabolizing lipids during the GV0-GV1 transition, which occurs during the early-to-middle stage of follicle development, and that the inability of GV0 oocytes to mature and develop into an embryo might depend, at least in part, from inappropriate capacity of the surrounding CC to metabolize lipids. Nevertheless, this hypothesis remains to be confirmed experimentally.

Gene expression profile in CC has attracted great interest in the last years. In fact, small biopsy of the cumulus oophorus could be easily collected before IVM, without perturbing oocyte viability, and assayed for expression of genes used as markers to predict corresponding oocyte’s quality. In this view, the present study confirms several previously reported markers associated with poor or high embryonic developmental potential in cattle, such as GATM or MAN1A1 (Bunel *et al.* , 2015, Bunel *et al.* , 2014). Notably, a similar approach has been conducted in the primed mouse model by comparing the transcriptomic profiles of CC isolated from antral oocytes with a Non Surrounded Nucleolus configuration (NSN, less compacted chromatin) and Surrounded Nucleolus configuration (SN, more compacted chromatin) (Vigone *et al.* , 2013, Zuccotti *et al.* , 1995). Compared to the present study in the cow, Vigone et al found a relatively low number of differentially expressed genes with fold changes higher than 2. The difference of the animal model of course could explain this difference. Moreover, we cannot exclude that taking

advantages of the gradual chromatin remodeling by considering two intermediate stages of compaction (GV1 and GV2) between the two extremes (GV0 and GV3) allowed the identification of a higher number of differentially expressed genes. It may be possible indeed that mouse oocytes with intermediated configurations (Bonnet-Garnier *et al.* , 2012, Bouniol-Baly *et al.* , 1999), which are generally grouped together with one of the two extremes may limit the capacity of revealing certain differences. On the other hand, we found correspondence with some of the genes identified by Vigone et al., such as Has2, which is up regulated in bovine CC_GV3 and mouse SN oocytes when compared to GV0 and NSN oocytes respectively. This set the stage for further comparative studies between the mouse and the bovine model.

Importantly, besides the assessment and confirmation of genes with known function in the reproductive system, our analysis provides multiple new biomarkers that are potentially involved in oocyte competence acquisition. For example, our data indicate that SLC39A8 is one of the genes whose expression constantly increases in CC during the GV0-to-GV3 transition. SLC39A8, also known as ZIP8, encodes for a member of the SLC39 family of solute-carrier genes, which shows structural characteristics of zinc transporters (Wang *et al.* , 2012). Recently, it has been shown that oocyte zinc content exerts important roles in oocyte function in mice, especially during meiotic maturation and fertilization (Bernhardt *et al.* , 2011, Bernhardt *et al.* , 2012, Kim *et al.* , 2011, Kim *et al.* , 2010, Kong *et al.* , 2012, Tian and Diaz, 2012). Moreover, Lisle et al. suggested that CC regulate the amount of free-Zinc in the oocyte during maturation (Lisle *et al.* , 2013). Interestingly, findings in mice show that acute dietary zinc deficiency during preconception (i.e. restricted to 3-5 days before ovulation) disrupts oocyte chromatin methylation and alters transcriptional regulation of repetitive elements, which is associated with severe defects of pre- and post-implantation embryonic development as well as of placental development (Tian *et al.* , 2014, Tian and Diaz, 2013). This is important since the period in which the mice were

fed with a zinc deficiency diet in these studies, corresponds to the final oocyte growth phase, when chromatin remodeling occurs (Albertini, 1992, Bonnet-Garnier *et al.*, 2012, Bouniol-Baly *et al.*, 1999, De La Fuente *et al.* , 2004, Debey *et al.* , 1993, Zuccotti *et al.*, 1995). These data clearly indicate that zinc plays important roles also before meiotic resumption and our data might set the stage for further investigation on the role of SLC39A8 as a possible player acting in the somatic compartment and involved in the control of oocyte zinc content, which is in turn important for the establishment of oocyte epigenetic signature. Interestingly, in the mouse model the zinc transporter SLC39A10 was found to be up regulated in CC from SN oocytes, when compared to NSN oocytes (Vigone *et al.*, 2013).

Importantly, besides the identification of single gene's function, the present dataset gives the opportunity to find pathways and mechanisms that are set in place in the somatic compartment that ultimately affect oocyte quality. This has paramount implications in the development of oocyte culture systems specifically formulated to fulfill the specific needs of the oocyte in a specific stage and support their in vitro development. For example, *in silico* analysis of differentially expressed genes in the three contrasts through IPA, revealed that apoptosis is predicted to be inhibited in CC of GV1 and of GV2 (even if at a lower extent) while it is predicted to be activated in CC of oocytes with the highest degree of chromatin compaction (GV3). Among the apoptosis related genes identified by IPA, angiopoietin 2 (ANGPT2) was the most up regulated gene in CC_GV3 when compared to CC_GV0, ANGPT2 is an antagonist of the angiogenic factor ANGPT1 that signals through the endothelial cell–specific Tie2 receptor tyrosine kinase. ANGPT2 disrupts the vascular remodeling ability of ANGPT1 and may induce endothelial cell apoptosis (Maisonpierre *et al.* , 1997). In the cyclic ovary, ANGPT1, ANGPT2 Tie1 and Tie2, play important roles in the modulation of vascular growth and regression (Goede *et al.* , 1998, Hazzard *et al.* , 1999, Wulff *et al.* , 2001a, Wulff *et al.* , 2000, Wulff *et al.* , 2001b) and studies in cow revealed a function of this system in the remodeling of the vascular network

specifically in the ovarian follicle (Hayashi *et al.* , 2003, Hayashi *et al.* , 2004). Strikingly, ANGPT2 was found to be up-regulated in early atretic follicles (Girard *et al.* , 2015, Hayashi *et al.*, 2003) thus supporting our finding that CC_GV3 are more prone to apoptosis.

These in silico predictions are experimentally confirmed by the facts that the CC's susceptibility to apoptosis increases with oocyte's chromatin compaction. Moreover these data are in agreement with previous findings indicating that functional gap-junction mediated communication between the oocyte and the surrounding CC is impaired in COC enclosing a GV3 oocyte and with signs of early cellular degeneration observed in GV3 oocytes at the ultrastructure level (Lodde *et al.*, 2007, Lodde *et al.*, 2008). On the other hand, the present findings support the general idea that COC enclosing a GV1 oocyte are in an earlier stage of oocyte differentiation. In fact, Class 1 COC, which was originally characterized as the one with no morphological signs of degeneration and lower developmental competence (Blondin and Sirard, 1995, Hazeleger *et al.*, 1995) and whose oocytes were found to be in an earlier stage of differentiation as assessed by BCB staining (present study), was the solely class enriched in GV1 oocytes.

On the basis of our findings we designed a tailored culture system, which confirmed that the success of in vitro cultural strategies aimed at improving oocyte developmental capability is 'stage dependent', i.e. mainly due to the characteristic of the COC that are subjected to the procedure. Indeed we demonstrated that standard IVM conditions are inappropriate to support pre-implantation embryonic development of GV1 enriched Class 1 COC, while their developmental competence is positively affected by a 6h period of inhibition of meiotic resumption through cAMP modulators. On the contrary, the same treatment negatively affected Class 1 and 2 COC developmental competences, which is consistent to the findings that these classes only contain GV2 and GV3 oocytes. This in turn confirms earlier studies in which prolonged Pre-IVM (24h) increased GV0 meiotic and developmental competencies

(Luciano *et al.*, 2011). These data are consistent with one of the concepts beyond pre-maturation strategies (Franciosi *et al.*, 2014, Gilchrist, 2011, Gilchrist *et al.* , 2016, Sirard, 2011, Smitz *et al.*, 2011) i.e. the prolongation of GJ-mediated communication between the somatic and germinal compartments is expected to be more effective in COC with a functional oocyte-CC coupling (as in GV0 and GV1 (Lodde *et al.*, 2007)).

An important finding of the present work is that, in naturally cycling animals, COC selection based on follicle size does not allow isolation of a homogeneous population in terms of chromatin configuration. This implies that at each follicular wave, GV1-to-GV2 transition, which marks the acquisition of a high embryonic developmental potential, occurs at almost any size as the growth of the follicle slows down before dominant follicle emergence and concomitantly with FSH level decrease (Adams *et al.*, 2008, Forde *et al.* , 2011). After the highest FSH level is attained in the preovulatory peak, the atretic events would start and GV2-to-GV3 transition eventually occurs. The timing of such sequence would fit the preparation of oocyte for ovulation or atresia, which requires chromatin compaction in both cases. This further confirms a previously postulated hypothesis that "*GV3 oocytes represent that proportion of gametes, which have reached a high developmental capability during follicular growth, and that, at the time of collection, were undergoing early events of atresia*" (Lodde *et al.*, 2007, Lodde *et al.*, 2008). These concepts are summarized in a tentative model illustrated in **Figure 8** which well correlate with an average competence of 33% and early atresia improving developmental potential (Blondin and Sirard, 1995). If each follicle would contain a GV2 stage oocyte at its plateau phase and such status would be permissive for further development, it would explain the extraordinary stable blastocyst rate observed with bovine IVM since 1995. The growing follicles would be mainly GV1, the plateau phase (low FSH) GV2 and the early atretic GV3 with respectively low, high and medium developmental competence.

In conclusion, our data support the idea that the synchrony between nuclear, cytoplasmic and molecular events is finely tuned during the final phase of oocyte

growth and demonstrate the necessity of a deep knowledge of the biological process occurring in cumulus cells during the final growth of the oocyte for the refinement of customized culture systems, which should consider the metabolic requirements of the heterogeneous population of oocytes that are submitted to IVM. This is mandatory to significantly improve assisted reproductive technologies. Very recently high similarity in the process of chromatin remodeling occurring in bovine and human immature oocytes that reflects a high cellular and molecular heterogeneity in human oocyte have been reported (Sanchez *et al.*, 2015). Thus the present work may have important consequences for human IVM in which the results are still suboptimal compared to conventional IVF (Coticchio *et al.* , 2012). In addition to avoiding the primary adverse effects caused by controlled ovarian stimulation, further improvements in IVM effectiveness and efficiency may help broaden the use of IVM for fertility preservation and in infertile patients.

Acknowledgements

The authors thank Dr. Marina Perri of the Health Veterinary Inspection service at INALCA spa, and Drs. Valentina Baruffini and Fabio Barbieri from University of Milan for technical support.

Authors' Roles

All authors contributed substantially to this manuscript. AML, VL and MAS designed the study; CD, VL, RL, ID, IT and AML executed experiments; CD, RL, VL, AML and MAS analyzed the data; VL, CD and AML wrote the manuscript. All authors revised and approved the final manuscript.

Supplementary data

Supplementary data are available at: ...

Funding

This work was supported in part by NSERC Strategic Network EmbryoGENE, Canada and in part by CIG - Marie Curie Actions FP7-Reintegration-Grants within the 7th European Community Framework Programme (Contract: 303640,"Pro-Ovum" to VL).

Conflict of Interest

None declared

Reference List

Aardema H, Lolicato F, van de Lest CH, Brouwers JF, Vaandrager AB, van Tol HT, Roelen BA, Vos PL, Helms JB, Gadella BM. Bovine cumulus cells protect maturing oocytes from increased fatty acid levels by massive intracellular lipid storage. *Biol Reprod* 2013;**88**: 164.

Adams GP, Jaiswal R, Singh J, Malhi P. Progress in understanding ovarian follicular dynamics in cattle. *Theriogenology* 2008;**69**: 72-80.

Albertini DF. Cytoplasmic microtubular dynamics and chromatin organization during mammalian oogenesis and oocyte maturation. *Mutat Res* 1992;**296**: 57-68.

Auclair S, Uzbekov R, Elis S, Sanchez L, Kireev I, Lardic L, Dalbies-Tran R, Uzbekova S. Absence of cumulus cells during in vitro maturation affects lipid metabolism in bovine oocytes. *Am J Physiol Endocrinol Metab* 2013;**304**: E599-613.

Bernhardt ML, Kim AM, O'Halloran TV, Woodruff TK. Zinc requirement during meiosis I-meiosis II transition in mouse oocytes is independent of the MOS-MAPK pathway. *Biol Reprod* 2011;**84**: 526-536.

Bernhardt ML, Kong BY, Kim AM, O'Halloran TV, Woodruff TK. A zinc-dependent mechanism regulates meiotic progression in mammalian oocytes. *Biol Reprod* 2012;**86**: 114.

Blazejczyk M, Miron M, Nadon R. FlexArray: A statistical data analysis software for gene expression microarrays. *Genome Quebec, Montreal, Canada* 2007.

Blondin P, Bousquet D, Twagiramungu H, Barnes F, Sirard MA. Manipulation of follicular development to produce developmentally competent bovine oocytes. *Biol Reprod* 2002;**66**: 38-43.

Blondin P, Sirard MA. Oocyte and follicular morphology as determining characteristics for developmental competence in bovine oocytes. *Mol Reprod Dev* 1995;**41**: 54-62.

Bonnet-Garnier A, Feuerstein P, Chebrout M, Fleurot R, Jan HU, Debey P, Beaujean N. Genome organization and epigenetic marks in mouse germinal vesicle oocytes. *Int J Dev Biol* 2012;**56**: 877-887.

Bouniol-Baly C, Hamraoui L, Guibert J, Beaujean N, Szollosi MS, Debey P. Differential transcriptional activity associated with chromatin configuration in fully grown mouse germinal vesicle oocytes. *Biol Reprod* 1999;**60**: 580-587.

Bunel A, Jorssen EP, Merckx E, Leroy JL, Bols PE, Sirard MA. Individual bovine in vitro embryo production and cumulus cell transcriptomic analysis to distinguish cumulus-oocyte complexes with high or low developmental potential. *Theriogenology* 2015;**83**: 228-237.

Bunel A, Nivet AL, Blondin P, Vigneault C, Richard FJ, Sirard MA. Cumulus cell gene expression associated with pre-ovulatory acquisition of developmental competence in bovine oocytes. *Reprod Fertil Dev* 2014;**26**: 855-865.

Coticchio G, Dal Canto M, Mignini Renzini M, Guglielmo MC, Brambillasca F, Turchi D, Novara PV, Fadini R. Oocyte maturation: gamete-somatic cells interactions, meiotic resumption, cytoskeletal dynamics and cytoplasmic reorganization. *Hum Reprod Update* 2015;**21**: 427-454.

Coticchio G, Dal-Canto M, Guglielmo MC, Mignini-Renzini M, Fadini R. Human oocyte maturation in vitro. *Int J Dev Biol* 2012;**56**: 909-918.

Culhane AC, Perriere G, Considine EC, Cotter TG, Higgins DG. Between-group analysis of microarray data. *Bioinformatics* 2002;**18**: 1600-1608.

De La Fuente R. Chromatin modifications in the germinal vesicle (GV) of mammalian oocytes. *Dev Biol* 2006;**292**: 1-12.

De La Fuente R, Eppig JJ. Transcriptional activity of the mouse oocyte genome: companion granulosa cells modulate transcription and chromatin remodeling. *Dev Biol* 2001;**229**: 224-236.

De La Fuente R, Viveiros MM, Burns KH, Adashi EY, Matzuk MM, Eppig JJ. Major chromatin remodeling in the germinal vesicle (GV) of mammalian oocytes is dispensable for global transcriptional silencing but required for centromeric heterochromatin function. *Dev Biol* 2004;**275**: 447-458.

Debey P, Szollosi MS, Szollosi D, Vautier D, Girousse A, Besombes D. Competent mouse oocytes isolated from antral follicles exhibit different chromatin organization and follow different maturation dynamics. *Mol Reprod Dev* 1993;**36**: 59-74.

Edgar R, Domrachev M, Lash AE. Gene Expression Omnibus: NCBI gene expression and hybridization array data repository. *Nucleic Acids Res* 2002;**30**: 207-210.

Eppig JJ. Oocyte control of ovarian follicular development and function in mammals. *Reproduction* 2001;**122**: 829-838.

Eppig JJ, Schultz RM, O'Brien M, Chesnel F. Relationship between the developmental programs controlling nuclear and cytoplasmic maturation of mouse oocytes. *Dev Biol* 1994;**164**: 1-9.

Forde N, Beltman ME, Lonergan P, Diskin M, Roche JF, Crowe MA. Oestrous cycles in Bos taurus cattle. *Anim Reprod Sci* 2011;**124**: 163-169.

Franciosi F, Coticchio G, Lodde V, Tessaro I, Modina SC, Fadini R, Dal Canto M, Renzini MM, Albertini DF, Luciano AM. Natriuretic peptide precursor C delays meiotic

resumption and sustains gap junction-mediated communication in bovine cumulus-enclosed oocytes. *Biol Reprod* 2014;**91**: 61.

Gilbert I, Scantland S, Dufort I, Gordynska O, Labbe A, Sirard MA, Robert C. Real-time monitoring of aRNA production during T7 amplification to prevent the loss of sample representation during microarray hybridization sample preparation. *Nucleic Acids Res* 2009;**37**: e65.

Gilbert I, Scantland S, Sylvestre EL, Dufort I, Sirard MA, Robert C. Providing a stable methodological basis for comparing transcript abundance of developing embryos using microarrays. *Mol Hum Reprod* 2010;**16**: 601-616.

Gilchrist RB. Recent insights into oocyte-follicle cell interactions provide opportunities for the development of new approaches to in vitro maturation. *Reprod Fertil Dev* 2011;**23**: 23-31.

Gilchrist RB, Lane M, Thompson JG. Oocyte-secreted factors: regulators of cumulus cell function and oocyte quality. *Hum Reprod Update* 2008;**14**: 159-177.

Gilchrist RB, Luciano AM, Richani D, Zeng HT, Wang X, Sugimura S, Smitz J, Richard FJ, Thompson JG. Oocyte maturation and quality: role of cyclic nucleotides. *Reproduction* 2016;**doi:** http://dx.doi.org/10.1530/REP-15-0606.

Girard A, Dufort I, Douville G, Sirard MA. Global gene expression in granulosa cells of growing, plateau and atretic dominant follicles in cattle. *Reprod Biol Endocrinol* 2015;**13**: 17.

Goede V, Schmidt T, Kimmina S, Kozian D, Augustin HG. Analysis of blood vessel maturation processes during cyclic ovarian angiogenesis. *Lab Invest* 1998;**78**: 1385-1394.

Gordon I. *Laboratory production of cattle embryos, 2nd Ed.*, 2003. CABI Publishing, Cambridge MA (USA).

Gougeon A. Dynamics of follicular growth in the human: a model from preliminary results. *Hum Reprod* 1986;**1**: 81-87.

Gougeon A. Regulation of ovarian follicular development in primates: facts and hypotheses. *Endocr Rev* 1996;**17**: 121-155.

Hayashi KG, Acosta TJ, Tetsuka M, Berisha B, Matsui M, Schams D, Ohtani M, Miyamoto A. Involvement of angiopoietin-tie system in bovine follicular development and atresia: messenger RNA expression in theca interna and effect on steroid secretion. *Biol Reprod* 2003;**69**: 2078-2084.

Hayashi KG, Berisha B, Matsui M, Schams D, Miyamoto A. Expression of mRNA for the angiopoietin-tie system in granulosa cells during follicular development in cows. *J Reprod Dev* 2004;**50**: 477-480.

Hazeleger NL, Hill DJ, Stubbing RB, Walton JS. Relationship of morphology and follicular fluid environment of bovine oocytes to their developmental potential in vitro. *Theriogenology* 1995;**43**: 509-522.

Hazzard TM, Molskness TA, Chaffin CL, Stouffer RL. Vascular endothelial growth factor (VEGF) and angiopoietin regulation by gonadotrophin and steroids in macaque granulosa cells during the peri-ovulatory interval. *Mol Hum Reprod* 1999;**5**: 1115-1121.

Hyttel P, Fair T, Callesen H, Greve T. Oocyte growth, capacitation and final maturation in cattle. *Theriogenology* 1997;**47**: 23-32.

Jolly PD, Tisdall DJ, Heath DA, Lun S, McNatty KP. Apoptosis in bovine granulosa cells in relation to steroid synthesis, cyclic adenosine 3',5'-monophosphate response

to follicle-stimulating hormone and luteinizing hormone, and follicular atresia. *Biol Reprod* 1994;**51**: 934-944.

Kim AM, Bernhardt ML, Kong BY, Ahn RW, Vogt S, Woodruff TK, O'Halloran TV. Zinc sparks are triggered by fertilization and facilitate cell cycle resumption in mammalian eggs. *ACS Chem Biol* 2011;**6**: 716-723.

Kim AM, Vogt S, O'Halloran TV, Woodruff TK. Zinc availability regulates exit from meiosis in maturing mammalian oocytes. *Nat Chem Biol* 2010;**6**: 674-681.

Kim JY, Kinoshita M, Ohnishi M, Fukui Y. Lipid and fatty acid analysis of fresh and frozen-thawed immature and in vitro matured bovine oocytes. *Reproduction* 2001;**122**: 131-138.

Kong BY, Bernhardt ML, Kim AM, O'Halloran TV, Woodruff TK. Zinc maintains prophase I arrest in mouse oocytes through regulation of the MOS-MAPK pathway. *Biol Reprod* 2012;**87**: 11, 11-12.

Kumar L, M EF. Mfuzz: a software package for soft clustering of microarray data. *Bioinformation* 2007;**2**: 5-7.

Labrecque R, Lodde V, Dieci C, Tessaro I, Luciano AM, Sirard MA. Chromatin remodelling and histone mRNA accumulation in bovine germinal vesicle oocytes. *Mol Reprod Dev* 2015;**82**: 450-462.

Landry DA, Bellefleur AM, Labrecque R, Grand FX, Vigneault C, Blondin P, Sirard MA. Effect of cow age on the in vitro developmental competence of oocytes obtained following FSH stimulation/coasting treatments. *Theriogenology* 2016.

Lisle RS, Anthony K, Randall MA, Diaz FJ. Oocyte-cumulus cell interactions regulate free intracellular zinc in mouse oocytes. *Reproduction* 2013;**145**: 381-390.

Lodde V, Franciosi F, Tessaro I, Modina SC, Luciano AM. Role of gap junction-mediated communications in regulating large-scale chromatin configuration remodeling and embryonic developmental competence acquisition in fully grown bovine oocyte. *J Assist Reprod Genet* 2013;**30**: 1219-1226.

Lodde V, Modina S, Galbusera C, Franciosi F, Luciano AM. Large-scale chromatin remodeling in germinal vesicle bovine oocytes: interplay with gap junction functionality and developmental competence. *Mol Reprod Dev* 2007;**74**: 740-749.

Lodde V, Modina S, Maddox-Hyttel P, Franciosi F, Lauria A, Luciano AM. Oocyte morphology and transcriptional silencing in relation to chromatin remodeling during the final phases of bovine oocyte growth. *Mol Reprod Dev* 2008;**75**: 915-924.

Lodde V, Modina SC, Franciosi F, Zuccari E, Tessaro I, Luciano AM. Localization of DNA methyltransferase-1 during oocyte differentiation, in vitro maturation and early embryonic development in cow. *Eur J Histochem* 2009;**53**: e24.

Lonergan P, Fair T. In vitro-produced bovine embryos: dealing with the warts. *Theriogenology* 2008;**69**: 17-22.

Luciano AM, Franciosi F, Dieci C, Lodde V. Changes in large-scale chromatin structure and function during oogenesis: a journey in company with follicular cells. *Anim Reprod Sci* 2014;**149**: 3-10.

Luciano AM, Franciosi F, Modina SC, Lodde V. Gap junction-mediated communications regulate chromatin remodeling during bovine oocyte growth and differentiation through cAMP-dependent mechanism(s). *Biol Reprod* 2011;**85**: 1252-1259.

Luciano AM, Lodde V. Changes of Large-Scale Chromatin Configuration During Mammalian Oocyte Differentiation. In Coticchio G, Albertini DF, De Santis L (eds) Oogenesis. 2013. Springer London, pp. 93-108.

Luciano AM, Lodde V, Beretta MS, Colleoni S, Lauria A, Modina S. Developmental capability of denuded bovine oocyte in a co-culture system with intact cumulus-oocyte complexes: role of cumulus cells, cyclic adenosine 3',5'-monophosphate, and glutathione. *Mol Reprod Dev* 2005;**71**: 389-397.

Luciano AM, Modina S, Gandolfi F, Lauria A, Armstrong DT. Effect of cell-to-cell contact on in vitro deoxyribonucleic acid synthesis and apoptosis responses of bovine granulosa cells to insulin-like growth factor-I and epidermal growth factor. *Biol Reprod* 2000;**63**: 1580-1585.

Lussier JG, Matton P, Dufour JJ. Growth rates of follicles in the ovary of the cow. *J Reprod Fertil* 1987;**81**: 301-307.

Maisonpierre PC, Suri C, Jones PF, Bartunkova S, Wiegand SJ, Radziejewski C, Compton D, McClain J, Aldrich TH, Papadopoulos N et al. Angiopoietin-2, a natural antagonist for Tie2 that disrupts in vivo angiogenesis. *Science* 1997;**277**: 55-60.

Matorras R, Ruiz JI, Mendoza R, Ruiz N, Sanjurjo P, Rodriguez-Escudero FJ. Fatty acid composition of fertilization-failed human oocytes. *Hum Reprod* 1998;**13**: 2227-2230.

Matzuk MM, Burns KH, Viveiros MM, Eppig JJ. Intercellular communication in the mammalian ovary: oocytes carry the conversation. *Science* 2002;**296**: 2178-2180.

Merton JS, de Roos AP, Mullaart E, de Ruigh L, Kaal L, Vos PL, Dieleman SJ. Factors affecting oocyte quality and quantity in commercial application of embryo technologies in the cattle breeding industry. *Theriogenology* 2003;**59**: 651-674.

Monniaux D, Clement F, Dalbies-Tran R, Estienne A, Fabre S, Mansanet C, Monget P. The ovarian reserve of primordial follicles and the dynamic reserve of antral growing follicles: what is the link? *Biol Reprod* 2014;**90**: 85.

Montani DA, Cordeiro FB, Regiani T, Victorino AB, Pilau EJ, Gozzo FC, Ferreira CR, Fraietta R, Lo Turco EG. The follicular microenviroment as a predictor of pregnancy: MALDI-TOF MS lipid profile in cumulus cells. *J Assist Reprod Genet* 2012;**29**: 1289-1297.

Nivet AL, Bunel A, Labrecque R, Belanger J, Vigneault C, Blondin P, Sirard MA. FSH withdrawal improves developmental competence of oocytes in the bovine model. *Reproduction* 2012;**143**: 165-171.

Pavlok A, Lucas-Hahn A, Niemann H. Fertilization and developmental competence of bovine oocytes derived from different categories of antral follicles. *Mol Reprod Dev* 1992;**31**: 63-67.

Robert C, Nieminen J, Dufort I, Gagne D, Grant JR, Cagnone G, Plourde D, Nivet AL, Fournier E, Paquet E et al. Combining resources to obtain a comprehensive survey of the bovine embryo transcriptome through deep sequencing and microarrays. *Mol Reprod Dev* 2011;**78**: 651-664.

Sanchez F, Romero S, De Vos M, Verheyen G, Smitz J. Human cumulus-enclosed germinal vesicle oocytes from early antral follicles reveal heterogeneous cellular and molecular features associated with in vitro maturation capacity. *Hum Reprod* 2015;**30**: 1396-1409.

Sirard MA. Follicle environment and quality of in vitro matured oocytes. *J Assist Reprod Genet* 2011;**28**: 483-488.

Smitz JE, Thompson JG, Gilchrist RB. The promise of in vitro maturation in assisted reproduction and fertility preservation. *Semin Reprod Med* 2011;**29**: 24-37.

Stringfellow D, A., Givens MD. *Manual of the International Embryo Transfer Society: a procedural guide and general information for the use of embryo transfer technology emphasizing sanitary procedures, 4th Ed.*, 2010. Savoy, IL (USA).

Su YQ, Sugiura K, Wigglesworth K, O'Brien MJ, Affourtit JP, Pangas SA, Matzuk MM, Eppig JJ. Oocyte regulation of metabolic cooperativity between mouse cumulus cells and oocytes: BMP15 and GDF9 control cholesterol biosynthesis in cumulus cells. *Development* 2008;**135**: 111-121.

Tian X, Anthony K, Neuberger T, Diaz FJ. Preconception zinc deficiency disrupts postimplantation fetal and placental development in mice. *Biol Reprod* 2014;**90**: 83.

Tian X, Diaz FJ. Zinc depletion causes multiple defects in ovarian function during the periovulatory period in mice. *Endocrinology* 2012;**153**: 873-886.

Tian X, Diaz FJ. Acute dietary zinc deficiency before conception compromises oocyte epigenetic programming and disrupts embryonic development. *Dev Biol* 2013;**376**: 51-61.

Torner H, Ghanem N, Ambros C, Holker M, Tomek W, Phatsara C, Alm H, Sirard MA, Kanitz W, Schellander K et al. Molecular and subcellular characterisation of oocytes screened for their developmental competence based on glucose-6-phosphate dehydrogenase activity. *Reproduction* 2008;**135**: 197-212.

Vandesompele J, De Preter K, Pattyn F, Poppe B, Van Roy N, De Paepe A, Speleman F. Accurate normalization of real-time quantitative RT-PCR data by geometric averaging of multiple internal control genes. *Genome Biol* 2002;**3**: RESEARCH0034.

Vassena R, Mapletoft RJ, Allodi S, Singh J, Adams GP. Morphology and developmental competence of bovine oocytes relative to follicular status. *Theriogenology* 2003;**60**: 923-932.

Vigone G, Merico V, Prigione A, Mulas F, Sacchi L, Gabetta M, Bellazzi R, Redi CA, Mazzini G, Adjaye J et al. Transcriptome based identification of mouse cumulus cell markers that predict the developmental competence of their enclosed antral oocytes. *BMC Genomics* 2013;**14**: 380.

Wang CY, Jenkitkasemwong S, Duarte S, Sparkman BK, Shawki A, Mackenzie B, Knutson MD. ZIP8 is an iron and zinc transporter whose cell-surface expression is up-regulated by cellular iron loading. *J Biol Chem* 2012;**287**: 34032-34043.

Wulff C, Wiegand SJ, Saunders PT, Scobie GA, Fraser HM. Angiogenesis during follicular development in the primate and its inhibition by treatment with truncated Flt-1-Fc (vascular endothelial growth factor Trap(A40)). *Endocrinology* 2001a;**142**: 3244-3254.

Wulff C, Wilson H, Largue P, Duncan WC, Armstrong DG, Fraser HM. Angiogenesis in the human corpus luteum: localization and changes in angiopoietins, tie-2, and vascular endothelial growth factor messenger ribonucleic acid. *J Clin Endocrinol Metab* 2000;**85**: 4302-4309.

Wulff C, Wilson H, Rudge JS, Wiegand SJ, Lunn SF, Fraser HM. Luteal angiogenesis: prevention and intervention by treatment with vascular endothelial growth factor trap(A40). *J Clin Endocrinol Metab* 2001b;**86**: 3377-3386.

Zuccotti M, Garagna S, Merico V, Monti M, Alberto Redi C. Chromatin organisation and nuclear architecture in growing mouse oocytes. *Mol Cell Endocrinol* 2005;**234**: 11-17.

Zuccotti M, Piccinelli A, Giorgi Rossi P, Garagna S, Redi CA. Chromatin organization during mouse oocyte growth. *Mol Reprod Dev* 1995;**41**: 479-485.

Figure Legends

Figure 1: Microarray analysis of cumulus cells isolated from oocytes with different large-scale chromatin configuration.

A: Experimental design. Cumulus cells (CC) associated to oocytes with GV0, GV1, GV2 and GV3 chromatin configuration were isolated and subjected to microarray analysis. The hybridizations were performed using a reference design, where cumulus cells isolated from oocytes with GV1, GV2 and GV3 chromatin configuration where compared with CC isolated from GV0 oocytes (CC_GV0 vs. CC_GV1; CC_GV0 vs. CC_GV2; CC_GV0 vs. CC_GV3). In each contrast the CC_GV0 group represents the reference group. Overall, 12 hybridizations corresponding to the four biological replicates and 3 comparisons were performed.

B: Venn's diagram showing commonly expressed probes in the four experimental groups. Diagram was generated using the online tool VENNY 2.0 (*Oliveros, J.C. (2007-2015) Venny. An interactive tool for comparing lists with Venn's diagrams.* http://bioinfogp.cnb.csic.es/tools/venny/index.html), in which was uploaded the lists of expressed probes in each group.

C: Between group analysis (BGA) of the cumulus cells microarray data, in which the samples are classified according to their transcriptomic profile (Culhane *et al.*, 2002) using the online tool available within the EmbryoGENE LIMS and Microarray Analysis (ELMA) pipeline. The plot illustrates the global distribution of transcriptome data (expressed probes) from the four experimental groups (cumulus cells from GV0, GV1, GV2 or GV3 oocytes) and the four biological replicates (dots in each group). The relative distance between each group indicates the global transcriptional differences among cumulus cells isolated from oocytes with different chromatin configurations.

Figure 2: Clusters analysis.

Graphs represent the sixteen clusters generated by the mFuzz clustering analysis (Kumar and M, 2007). For each cluster the number of statistically significant probes that best fit to each profile is indicated between brackets. Note: cluster 6 is the one with the higher number of best fit probes.

Figure 3: Quantitative reverse-transcriptase-PCR (qRT-PCR) validation of the microarray results.

Validation of microarray data by means of qRT-PCR. Graphs indicate relative expression levels of selected genes in cumulus cells isolated from oocytes with GV0, GV1, GV2 or GV3 chromatin configuration; expression levels for each gene were normalized using ACTB, GAPDH and HPRT1 as reference genes. Relative fold changes were calculated using the delta-delta Ct method using CC_GV0 as reference group. Data were analyzed by one-way ANOVA followed by Newman-Keuls multiple comparison test and are expressed as means ± SEM. Different superscripts indicate significant differences between groups ($p<0.05$). Where applicable, test for linear trend was also conducted (*, $p<00.5$)
Note: selected genes, with accession number, primer sequences, annealing temperature and product size as **Supplemental table 1**

Figure 4: Functional analysis

IPA generated diagrams representing deregulated apoptosis-related genes ($p<0.05$; fold change higher than ±2) in CC_GV0 vs. CC_GV1 (A), CC_GV0 vs. CC_GV2 (B) and CC_GV0 vs. CC_GV3. Note that apoptosis is predicted to be inhibited (blue) in CC_GV1 and CC_GV2, while it is activated (orange) in CC_GV3. Gene lists are provided as supplemental table; genes in red are up-regulated; Genes in green are down-regulated.

Figure 5: Assessment of Caspase activity in cells isolated from oocytes with different chromatin configuration

CC associated to oocytes with GV0, GV1, GV2 and GV3 chromatin configuration were isolated and assayed for Caspase activity after 3h of culture using the CaspaTag™ Pan-Caspase In Situ Assay Kit. **A)** Representative pictures showing active Caspase in cells undergoing apoptosis and negative (arrows) cells. **B)** Graph shows the percentage of Caspase-active cells in each GV category; Data from 3 independent experiments were analyzed by one-way ANOVA followed by Newman-Keuls multiple comparison test; data are expressed as means ± SEM; a,b,c: different superscript indicate significant differences between groups ($p<0.05$).

Figure 6: Relationship between large-scale chromatin configuration, follicle size, COC morphology and oocyte glucose-6-phosphate dehydrogenase (G6PDH) activity

A) COC were collected from follicles of different diameter and chromatin configuration was assessed after cumulus cells removal. Graphs show the frequency of GV1, GV2 and GV3 chromatin configuration in each follicle size category. A total of 277 oocytes (167, 52 and 52 from small, medium and large antral follicle respectively), were used in this study in 3 independent experiments. Data were analyzed by one-way ANOVA. **B)** After collection, COC were separated according to morphological criteria as shown in the representative pictures (Class 1: homogeneous ooplasm and absence of expansion of outer layer cumulus cells; Class 2: minor granulation of the ooplasm and/or beginning of expansion of outer layer cumulus cells; Class 3: highly granulated ooplasm and few cumulus cells layers showing expansion). After classification, cumulus cells were removed and chromatin configuration was assessed. Graphs show the frequency of GV1, GV2 and GV3 chromatin configuration in each class. A total of 300 oocytes (101 Class 1, 119 Class 2 and 80 Class 3) were used in this study in 3 independent experiments. Data were

analyzed by one-way ANOVA followed by Newman-Keuls multiple comparison test; a,b, different letters indicate significant differences, $p<0.05$). **C)** After collection, COC were separated into Class 1 and Class 2/3 on the basis of their morphology and subjected to Brilliant Cresyl Blue staining (BCB). After removal of cumulus cells, oocytes were classified as BCB+ or BCB- as shown in the representative picture. Graph shows the percentage of BCB+ and BCB- oocytes in Class 1 and 2/3 COC. A total of 337 COC were analyzed (126 Class 1 and 211 of Class 2/3) in 9 independent experiments. Data were analyzed by one way ANOVA followed by Newman-Keuls multiple comparison test; data are expressed as means ± SEM; a, b, c, d different letters indicate significant differences ($p<0.05$).

Figure 7: Effect of pre-maturation treatment on COC with different morphology

After collection, COC were separated into Class 1 and Class 2/3 on the basis of their morphology and in vitro matured with or without the Pre-IVM treatment. Then oocytes were in vitro fertilized and in vitro cultured for 8 days. Groups of unsorted COC (mix of Class 1/2/3) were subjected to the same experimental procedure and used as controls. Graphs show the effect of the pre-IVM treatment on the blastocyst rate (**A**) and mean cell number per blastocyst (**B**). A total of 947 oocytes were analyzed in this study (292 mixed oocytes, 321 Class 1 and 334 Class 2/3) in 6 independent experiments. Data were analyzed by one way ANOVA followed by Newman-Keuls multiple comparison test; data are expressed as means ± SEM; a, b, different letters indicates significant differences ($p<0.05$).

Figure 8: Chromatin remodeling during follicular development: a model.

The figure shows chromatin remodeling, as it would occur during bovine estrous cycle. Follicles with white oocytes are non-atretic; with pink oocytes are early atretic and with purple oocytes are atretic. The growing follicles would be mainly GV1, the

plateau phase mainly GV2 and the early atretic GV 3. Adapted from Merton et al., 2003 (Merton *et al.*, 2003).

Tables:

Table 1: Number of differentially expressed probes (p<0.05)

	Total	Fold change > 2	Fold change > -2
CC_GV0 vs. CC_GV1	112	77	35
CC_GV0 vs. CC_GV2	127	42	85
CC_GV0 vs. CC_GV3	204	82	122

1170

Table 2: Molecular and Cellular Functions of best fit genes in most represented clusters identified by IPA (p<0.05)

Molecular and Cellular Functions	***p* Value**	**#Molecules**
Cluster 1 (↘↘↘) *(constant decrease from CC_GV0 to CC_GV3)*		
Cell Cycle	1.73E-02 - 3.49E-09	74
Cellular Assembly and Organization	1.73E-02 - 3.49E-09	48
DNA Replication, Recombination, and Repair	1.73E-02 - 3.49E-09	67
Cellular Movement	1.73E-02 - 5.10E-06	30
Cell Death and Survival	1.73E-02 - 6.41E-06	99
Cluster 5 (↗↗↗) *(constant increase from CC_GV0 to CC_GV3)*		
RNA Post-Transcriptional Modification	1.24E-02 - 2.06E-05	17
Protein Synthesis	8.88E-03 - 3.87E-05	43
Gene Expression	1.88E-02 - 5.04E-05	72
Cell Signaling	1.88E-02 - 3.43E-04	15
Vitamin and Mineral Metabolism	1.88E-02 - 3.43E-04	8
Cluster 6 (↘→→) *(down regulation between CC_GV0 and CC_GV1 and relatively stable low levels in successive groups)*		
Lipid Metabolism	2.16E-02 - 8.40E-05	103
Small Molecule Biochemistry	2.23E-02 - 8.40E-05	141
Cellular Assembly and Organization	2.13E-02 - 2.01E-04	60
Cellular Development	2.31E-02 - 2.23E-04	176
Cellular Growth and Proliferation	2.31E-02 - 2.23E-04	260
Cluster 9 (↗→→) (up regulation between CC_GV0 and CC_GV1 and relatively stable levels in successive groups)		
Lipid Metabolism	1.97E-02 - 2.65E-05	32
Small Molecule Biochemistry	1.97E-02 - 2.65E-05	46
Molecular Transport	1.97E-02 - 2.81E-05	69
Cellular Assembly and Organization	1.97E-02 - 1.22E-04	31
Cellular Function and Maintenance	1.97E-02 - 1.22E-04	37
Cluster 12 (↗↗→) (up regulation from CC_GV0 to CC_GV2 and relatively stable levels from CC_GV2 to CC_GV3)		
Lipid Metabolism	2.18E-02 - 8.79E-05	49
Small Molecule Biochemistry	2.18E-02 - 8.79E-05	71
Vitamin and Mineral Metabolism	2.15E-02 - 8.79E-05	23
Cell-To-Cell Signaling and Interaction	2.15E-02 - 8.79E-05	59
Cellular Movement	1.86E-02 - 9.96E-05	43

Table 3: Molecular and Cellular Functions identified by IPA (p<0.05, fold change higher than ± 2) in each contrast (CC_GV0 vs. CC_GV1, CC_GV0 vs. CC_GV2, CC_GV0 vs. CC_GV3)

Molecular and Cellular Functions	*p* Value	#Molecules
CC_GV0 vs. CC_GV1		
Cell Death and Survival	4.23E-03 - 2.69E-08	60
Cellular Function and Maintenance	4.28E-03 - 3.48E-07	64
Cellular Movement	4.31E-03 - 5.75E-07	42
Cellular Growth and Proliferation	3.51E-03 - 7.05E-07	63
Cell-To-Cell Signaling and Interaction	4.17E-03 - 9.85E-07	49
CC_GV0 vs. CC_GV2		
Cell Death and Survival	7.77E-03 - 2.51E-08	73
Cellular Function and Maintenance	8.19E-03 - 4.69E-08	60
Cellular Growth and Proliferation	7.51E-03 - 5.65E-07	76
Cellular Movement	7.72E-03 - 9.42E-07	49
Cell Morphology	8.19E-03 - 1.12E-05	53
CC_GV0 vs. CC_GV3		
Cell Death and Survival	1.78E-03 - 1.22E-15	107
Cellular Development	1.95E-03 - 7.66E-11	109
Cell Cycle	1.78E-03 - 1.10E-10	61
Cellular Growth and Proliferation	1.95E-03 - 1.25E-10	114
Cell Morphology	1.70E-03 - 1.16E-08	67

Supplemental material

Supplemental table 1

Gene name	Full name (accession number)	Primers sequence (5'-3')	Ann. Temp (°C)	Prod size (bp)
THBS1	Thrombospondin 1 (GeneID:281530)	F-ggaaagtgtttgagagcaggt R-gcacaagggatgggataaga	57	233
Serpine 2	Serpine 2 (GeneID:282521)	F- tgcattactttgggggtagaa R- cacaaatgcaaatccaaagag	53	188
RGS2	Regulator of G-protein signaling 2 (GeneID:513055)	F-gccgaaaagactgaccttga R-gaggccacataatcccagac	57	277
INHA	inhibin, alpha (GeneID:281254)	F- caccctcccagtttcatctt R- ggttgggcaccatctcatac	57	229
SLC39A8	solute carrier family 39 (zinc transporter), member 8 (GeneID:508193)	F-tgaacatcctagccccaatc R-tgacacaatacaaggtttcaaagg	57	250
GAPDH	glyceraldehyde-3-phosphate dehydrogenase (Gene ID: 281181)	F-ccaacgtgtctgttgtggatctga R-gagcttgacaaagtggtcgttgag	58	217
ACTB	actin, beta (Gene ID: 280979)	F- tgaaccctaaggccaaccgtg R-tgtagccacgctcggtcagga	59	267
HPRT1	hypoxanthine phosphoribosyltransferase 1 (Gene ID: 281229)	F-ggctcgagatgtgatgaagg R-gcaaagtctgcattgtcttcc	57	293

Supplemental table 2

1205

Gene lists of deregulated apoptosis-related genes (p<0.05; fold change higher than ± 2) shown in Figure 4

CC_GV0 vs. GV1		CC_GV0 vs. GV2		CC_GV0 vs. GV3	
Gene name	Fold change	Gene name	Fold change	Gene name	Fold change
FN1	5.560	GFRA1	3.460	ANGPT2	4.451
ANGPT2	4.075	ANGPT2	3.455	PLA2G7	3.333
SERPINE1	3.807	GRIK5	3.013	NEDD9	3.090
OLR1	3.502	TCF21	2.937	CTGF	3.038
LMO2	3.352	LMO2	2.846	GFRA1	2.985
GRIK5	2.925	PLA2G7	2.788	JMJD1C	2.733
SPRY2	2.881	SPRY2	2.723	HSPA1A	2.636
SPP1	2.836	LHX2	2.632	BAG3	2.635
PDGFRA	2.806	JMJD1C	2.443	LHX2	2.631
PLA2G7	2.782	IRF1	2.432	MAP3K5	2.535
GFRA1	2.665	INHA	2.360	PDGFRA	2.426
CTGF	2.623	MTMR9	2.221	SPRY2	2.394
TCF21	2.525	CTSC	2.183	APOA1	2.367
LHX2	2.448	NEDD9	2.122	PPP2R2A	2.347
IRF8	2.381	PDGFRA	2.104	LMO2	2.328
JMJD1C	2.278	MOBKL2B	2.072	SGMS2	2.323
NEDD9	2.248	CD47	2.067	GADD45A	2.322
PDXK	2.237	OLR1	2.051	CSNK1A1	2.270
B2M	2.198	ANXA4	2.041	TCF21	2.261

PLAT	2.128	APOA1	2.039	MAP3K8	2.258
FRZB	2.110	THPO	2.028	IRF1	2.244
CYP11A1	2.065	B2M	2.021	RB1	2.234
MSRB3	2.051	EMX2	-2.010	CD36	2.199
IRF1	2.033	RPRM	-2.030	HAS2	2.174
BAG3	2.032	DAB2	-2.037	ITGA2	2.159
MOBKL2B	2.030	EMILIN2	-2.046	SIAH1	2.141
F2	2.022	LUM	-2.058	ANXA4	2.141
ENC1	2.003	RRM2	-2.092	EIF2AK2	2.139
APOA1	2.001	GML	-2.102	CD47	2.119
DDIT4	-2.034	TCEB3	-2.176	SETX	2.117
CD99	-2.121	JUN	-2.177	MSRB3	2.105
SFRS2	-2.132	EPHX1	-2.229	GRIK5	2.100
DAB2	-2.137	TRAF1	-2.246	INHA	2.060
RRM2	-2.164	NR4A1	-2.250	MCL1	2.055
GML	-2.165	DCN	-2.286	ETS2	2.036
NAIP	-2.215	SFRS2	-2.320	SHISA5	2.026
GADD45B	-2.344	FBN1	-2.327	LMO4	2.026
TLR6	-2.430	PRKD2	-2.335	B2M	2.022
ATP1A2	-2.476	DUSP1	-2.353	SREBF2	2.015
SEPT4	-2.652	ID3	-2.381	NDEL1	2.011
HSPD1	-2.669	NAA35	-2.387	IGF2	-2.016
PTN	-2.687	GADD45G	-2.479	LUM	-2.022
TYRO3	-2.745	FOSB	-2.520	GIMAP5	-2.034
DNAJB1	-2.780	HSPD1	-2.656	TCEB3	-2.062
NAA35	-2.793	ATP1A2	-2.751	BUB1	-2.071
GSTA1	-3.312	DNAJB1	-2.756	GADD45B	-2.096

ATP6V1G2	-3.323	SEPT4	-2.780	TLR6	-2.098
EGR1	-3.328	CD99	-2.894	CCNB1	-2.117
TXNIP	-3.429	PTN	-2.956	FASTK	-2.145
KRT8	-3.648	TYRO3	-3.277	AURKB	-2.147
		ZFP36L1	-3.310	NUSAP1	-2.187
		GADD45B	-3.411	LGALS1	-2.213
		NAIP	-3.478	EMILIN2	-2.219
		TXNIP	-3.740	MAD2L2	-2.281
		GSTA1	-3.798	KIF18A	-2.292
		EGR1	-4.944	SMAD6	-2.298
		KRT8	-5.143	MST1	-2.301
		AXL	-5.851	DCN	-2.303
				CUL2	-2.306
				ATP6V1G2	-2.369
				PTTG1	-2.381
				TGFB3	-2.381
				SFRS2	-2.424
				TRAF1	-2.447
				CKAP2	-2.495
				NAIP	-2.585
				DDIT4	-2.612
				JUN	-2.637
				EMX2	-2.737
				TYRO3	-2.745
				FOSB	-2.827
				RRM2	-2.838
				NR4A1	-2.867

				CHEK1	-2.915
				NAA35	-2.945
				HSPD1	-2.950
				FOS	-2.964
				DNAJB1	-2.966
				ZFP36L1	-3.078
				TXNIP	-3.187
				PTN	-3.210
				ATP1A2	-3.299
				SEPT4	-3.379
				GSTA1	-3.402
				ID3	-3.427
				ZFP36	-3.467
				FBN1	-3.573
				DAB2	-3.651
				CD99	-3.924
				KRT8	-4.254
				AXL	-5.170
				DUSP1	-6.608
				EGR1	-7.186

1210

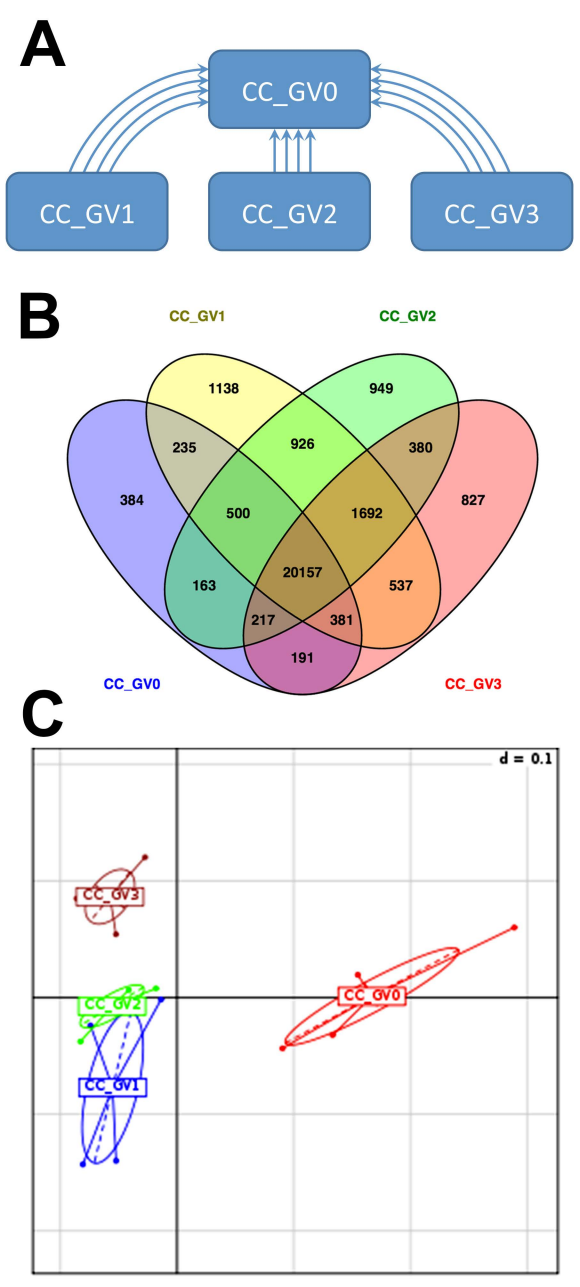
A
CC_GV0
CC_GV1
CC_GV2
CC_GV3
B
CC_GV1
CC_GV2
1138
949
235
926
380
384
500
1692
827
163
20157
537
217
381
191
CC_GV0
CC_GV3
C
d = 0.1
CC_GV3
CC_GV2
CC_GV0
CC_GV1

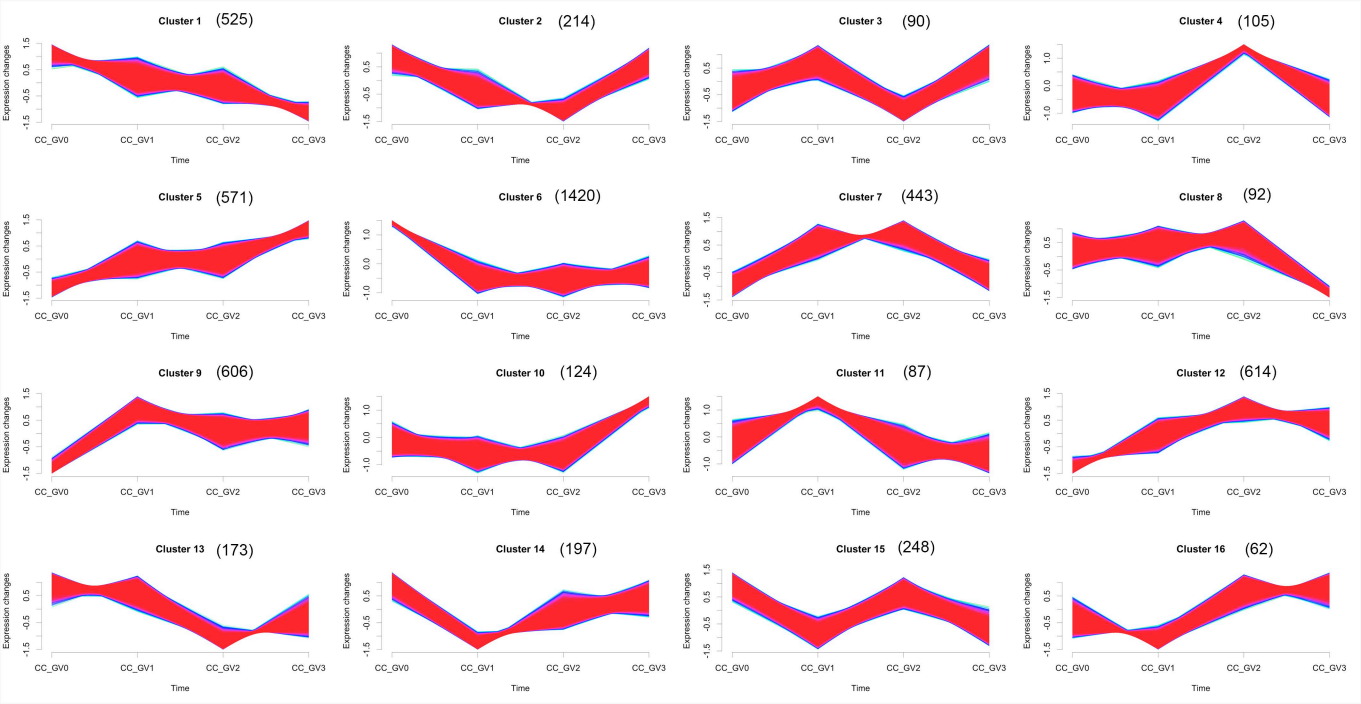
Cluster 1 (525)
Cluster 2 (214)
Cluster 3 (90)
Cluster 4 (105)
Cluster 5 (571)
Cluster 6 (1420)
Cluster 7 (443)
Cluster 8 (92)
Cluster 9 (606)
Cluster 10 (124)
Cluster 11 (87)
Cluster 12 (614)
Cluster 13 (173)
Cluster 14 (197)
Cluster 15 (248)
Cluster 16 (62)
Expression changes
Time
CC_GV0
CC_GV1
CC_GV2
CC_GV3

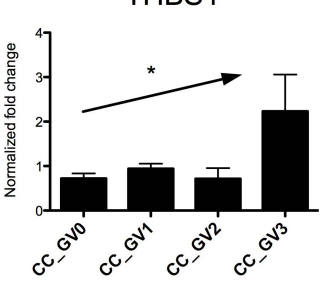
THBS1
Normalized fold change
4
3
2
1
0
*
CC_GV0
CC_GV1
CC_GV2
CC_GV3

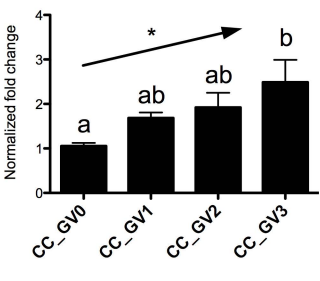
Serpine 2
Normalized fold change
4
3
2
1
0
*
a
ab
ab
b
CC_GV0
CC_GV1
CC_GV2
CC_GV3

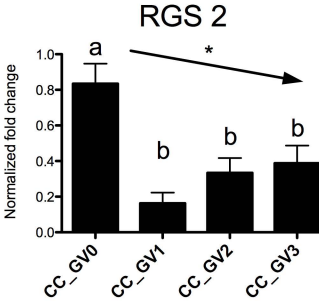
RGS 2
Normalized fold change
1.0
0.8
0.6
0.4
0.2
0.0
*
a
b
b
b
CC_GV0
CC_GV1
CC_GV2
CC_GV3

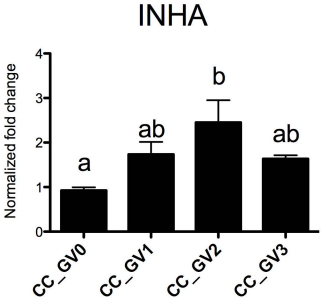
INHA
Normalized fold change
4
3
2
1
0
a
ab
b
ab
CC_GV0
CC_GV1
CC_GV2
CC_GV3

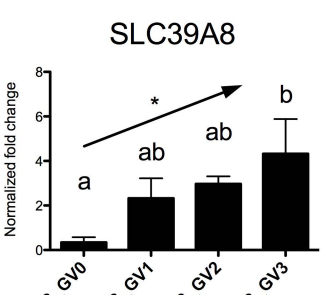
SLC39A8
Normalized fold change
8
6
4
2
0
*
a
ab
ab
b
CC_GV0
CC_GV1
CC_GV2
CC_GV3

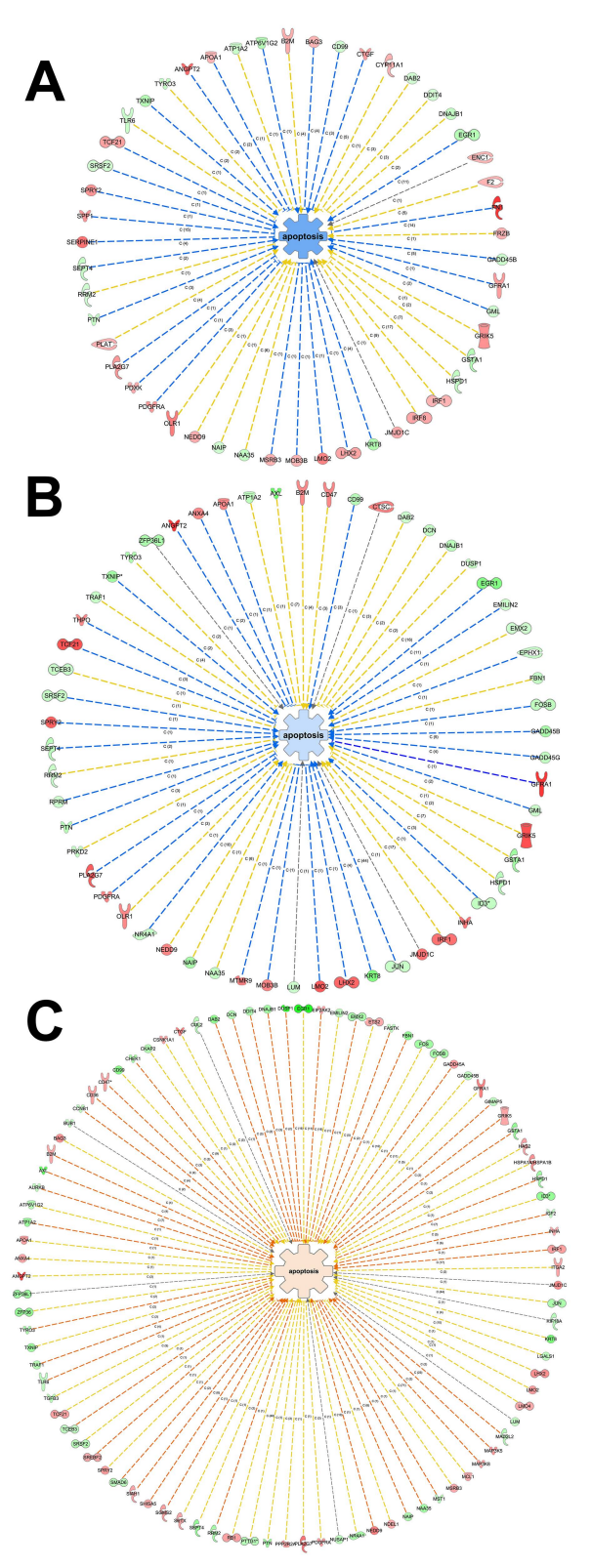
A
apoptosis
B
apoptosis
C
apoptosis
Legend
Enzyme
Growth factor
Ion Channel
Kinase
Ligand-dependent Nuclear Receptor
Phosphatase
Legend
Transcription Regulator
Transmembrane Receptor
Transporter
Other
Function
Relationship

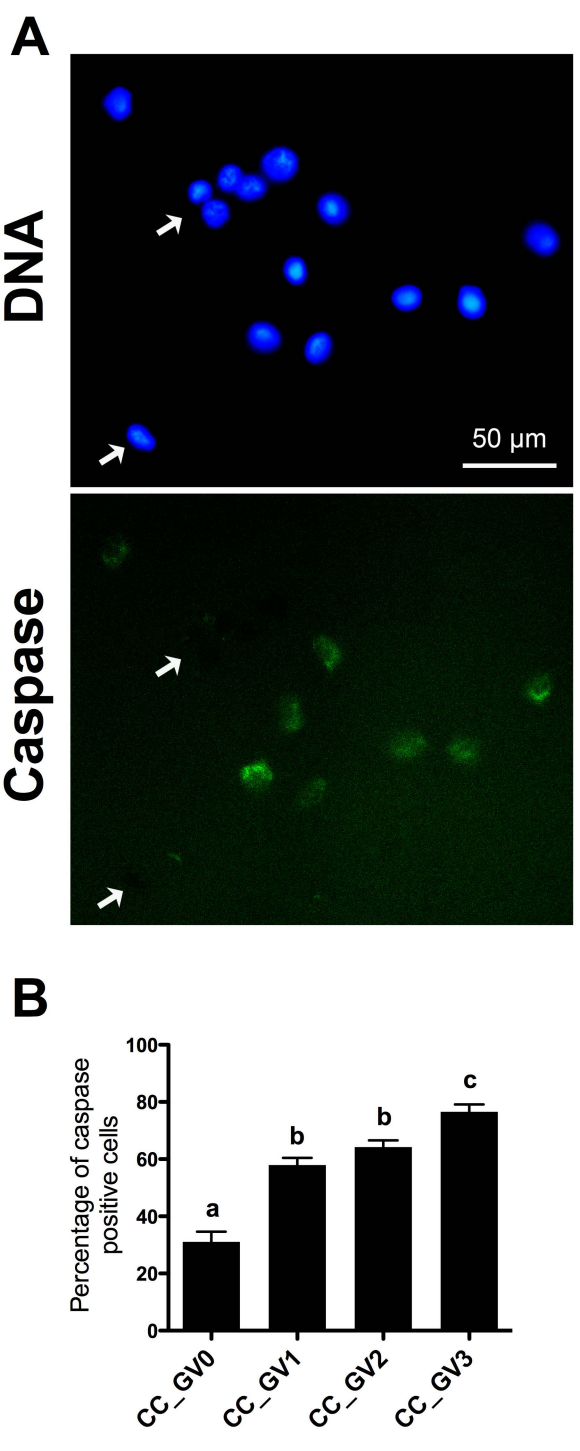
A
DNA
50 µm
Caspase
B
Percentage of caspase positive cells
100
80
60
40
20
0
a
b
b
c
CC_GV0
CC_GV1
CC_GV2
CC_GV3

A

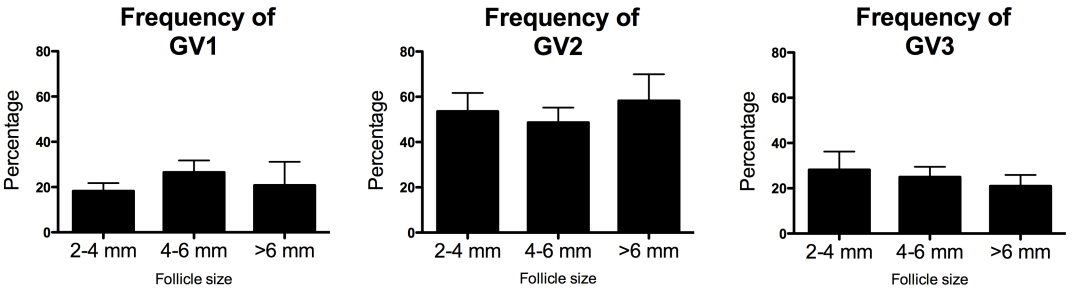
Frequency of GV1
Percentage
0
20
40
60
80
2-4 mm
4-6 mm
>6 mm
Follicle size
Frequency of GV2
Percentage
0
20
40
60
80
2-4 mm
4-6 mm
>6 mm
Follicle size
Frequency of GV3
Percentage
0
20
40
60
80
2-4 mm
4-6 mm
>6 mm
Follicle size

B

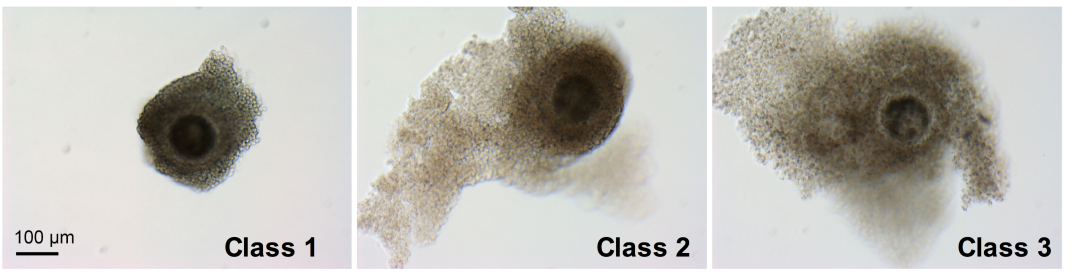
100 µm
Class 1
Class 2
Class 3

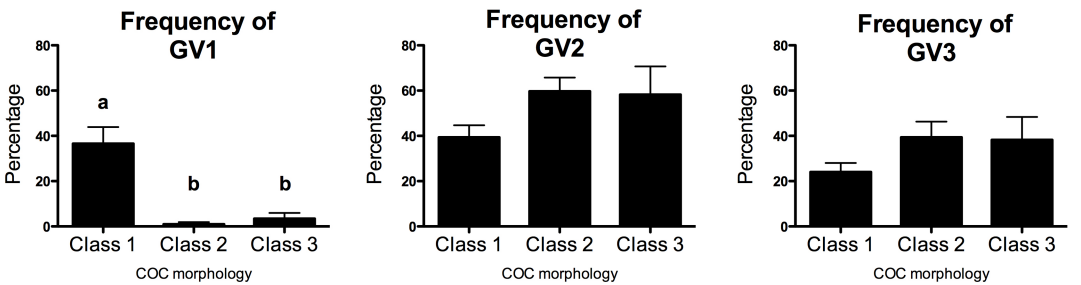
Frequency of GV1
Percentage
0
20
40
60
80
a
b
b
Class 1
Class 2
Class 3
COC morphology
Frequency of GV2
Percentage
0
20
40
60
80
Class 1
Class 2
Class 3
COC morphology
Frequency of GV3
Percentage
0
20
40
60
80
Class 1
Class 2
Class 3
COC morphology

C

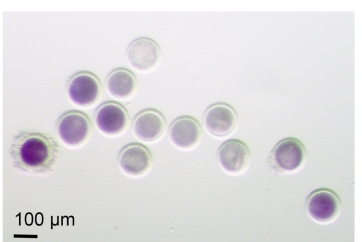
100 µm

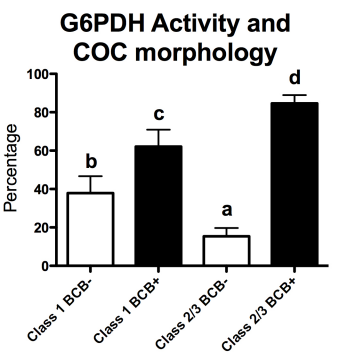
G6PDH Activity and COC morphology
Percentage
0
20
40
60
80
100
b
c
a
d
Class 1 BCB-
Class 1 BCB+
Class 2/3 BCB-
Class 2/3 BCB+

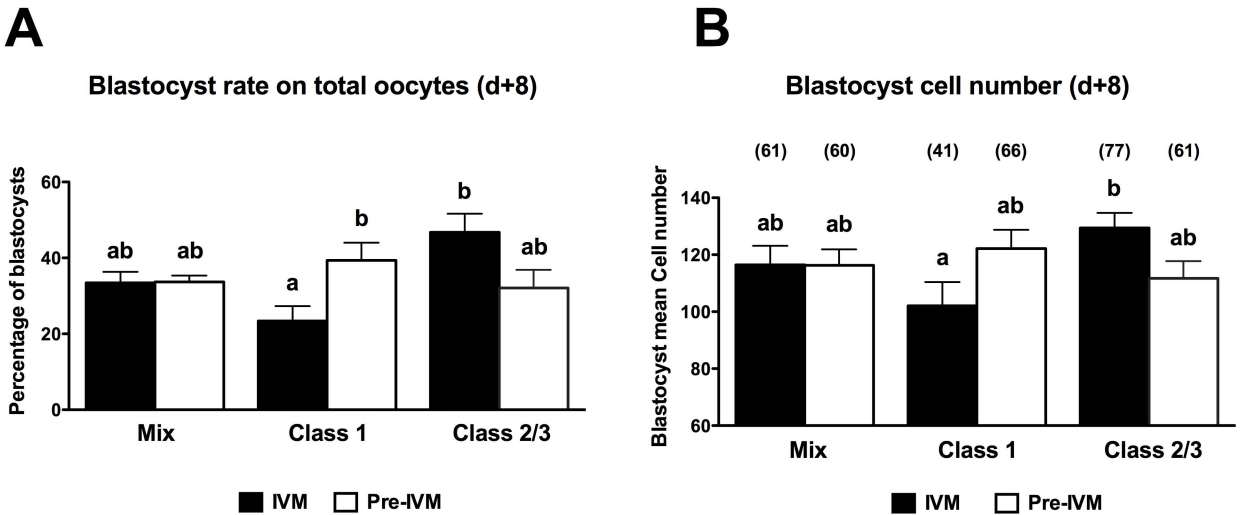
A
Blastocyst rate on total oocytes (d+8)
Percentage of blastocysts
60
40
20
0
ab
ab
a
b
b
ab
Mix
Class 1
Class 2/3
IVM
Pre-IVM
B
Blastocyst cell number (d+8)
Blastocyst mean Cell number
140
120
100
80
60
(61)
(60)
(41)
(66)
(77)
(61)
ab
ab
a
ab
b
ab
Mix
Class 1
Class 2/3
IVM
Pre-IVM

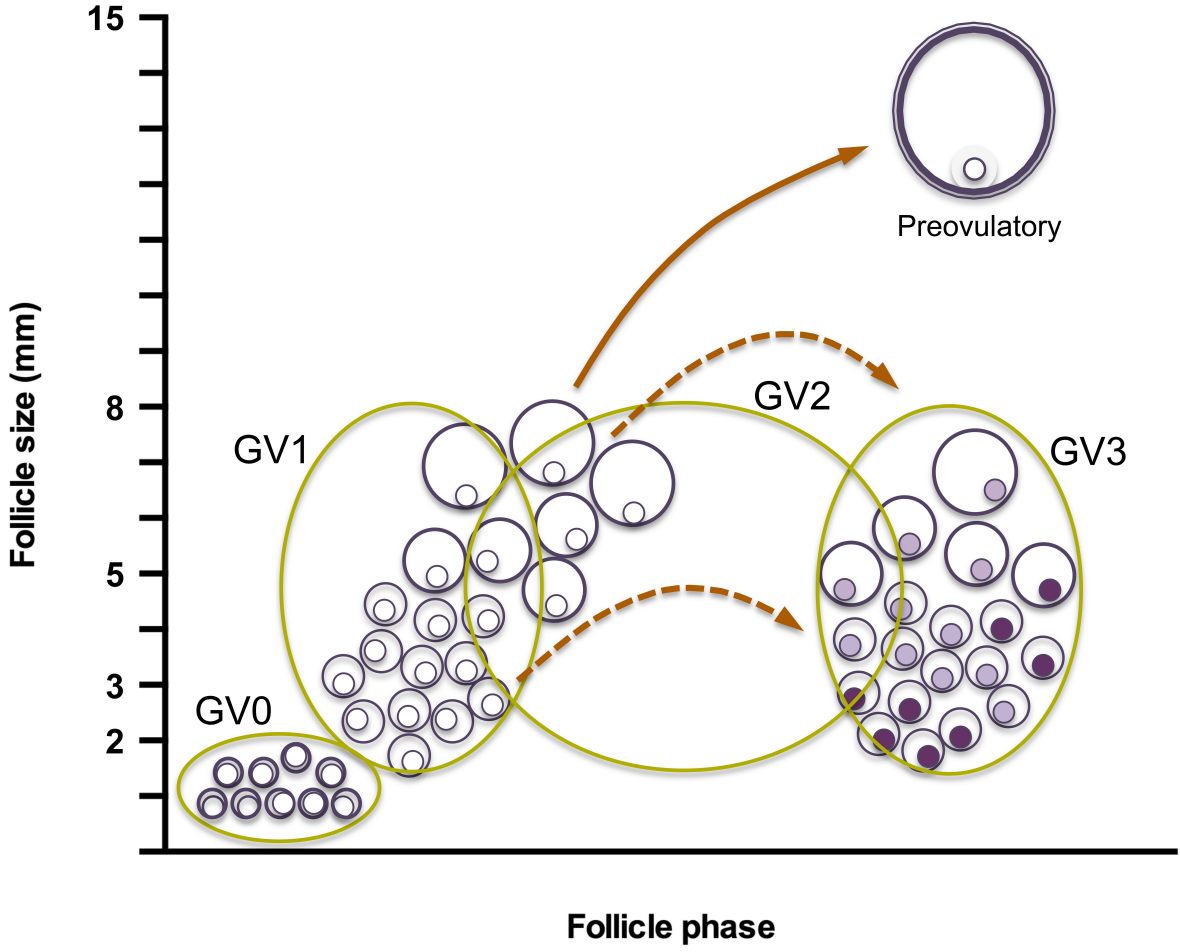
15
8
5
3
2
Follicle size (mm)
Preovulatory
GV1
GV2
GV3
GV0
Follicle phase